VOT 78371

A NOVEL TISSUE IMAGING METHOD USING SHORT PULSE MAGNETO ACOUSTIC WAVE

ISMAIL BIN ARIFFIN

FAKULTI KEJURUTERAAN ELEKTRIK

2011

A NOVEL TISSUE IMAGING METHOD USING SHORT PULSE MAGNETO ACOUSTIC WAVE

(KAEDAH PENGIMEJAN TISU MENGGUNAKAN GELOMBANG PENDEK MAGNETO AKUSTIK)

ISMAIL BIN ARIFFIN

EKO SUPRIYANTO

MAHEZA IRNA MOHAMAD SALIM

JABATAN KEJURUTERAAN ELEKTRONIK

FAKULTI KEJURUTERAAN ELEKTRIK

UNIVERSITI TEKNOLOGI MALAYSIA

2011

To my Family and Friends,

DEDICATION

Praised be to Allah, Who has granted me the strength and faith in completing this research. Peace and blessing of Allah are due to His Messenger, the prophet Muhammad and his family.

First of all, I would like to express my gratitude to the following organization and people who has helped me so much in completing this research:

- Ministry of Higher Education Malaysia for awarding me the Fundamental Research Grant Scheme (FRGS), without which this expansion of knowledge in the field of medical imaging cannot be conducted.
- Universiti Teknologi Malaysia especially Research Management Center for their assistance in managing and monitoring the progress of this research grant.
- Animal Ethics Committee, Universiti Kebangsaan Malaysia for allowing this research to register for animal ethics approval.
- My Co-researchers, who have dedicated their knowledge and expertise in the accomplishment of this research.
- My research assistants and students for their help in literature study, experimental setup, data collection, analysis, and finally the writing stage.
- Most importantly, my parents and my family for their countless loves, strong faith, prayers, encouragement and never ending support to me. I am deeply indebted to all the personal sacrifications and sincerity that I could never repay. This report is dedicated in remembering the hard works of everybody in making this research meaningful.

ABSTRACT

Breast cancer is one of the most common cancers and the leading cause of cancer death among women worldwide. Breast cancer incidence is increasing over the years with more than 1 million new cases reported each year. In addition to that, an average of 373000 women died globally every year in conjunction to the disease. In Malaysia, National Cancer Registry report for the year 2003-2005 states that, the incidence rate of breast cancer in Malaysian population is 47.4 per 100000 populations with Chinese is at the highest rate of 59.9, followed by Indian at 54.2 and Malay at 34.9 per 100000 populations. With the yearly increasing trend, improvement in diagnosis and treatment method is desirable to increase survival rate.

In the current medical practice, the goal of breast ultrasound imaging in breast cancer diagnostic is to achieve a more specific conclusion following a suspicious mammographic finding and to prevent unnecessary biopsies to find breast cancers missed by mammography. However, the sensitivity of ultrasound imaging in breast cancer detection is so much lower. This limits ultrasound imaging from taking a dominant role in breast screening. Tough ultrasonography has been declares as the current mainstay in breast cancer diagnosis, studies show that the proportion of patient in whom breast ultrasonography is considered necessary is only 40%. This means that, ultrasonography is not indicated for the rest 60% of patients referred for breast imaging. This practice explains major constraint of ultrasonography in breast imaging that limits its usage for diagnostic of breast symptoms and for screening asymptomatic patients. Hence, innovation to ultrasound imaging is very crucial so that this modality is capable

to explore and manipulate additional properties of breast cancer for better discrimination result.

Therefore, a hybrid imaging method that combines ultrasound and magnetism has been developed in this study. The aim is to create an imaging platform that is capable to access the acoustic and bioelectric properties of breast tissue for cancer detection. In Hybrid Magnetoacoustic Method (HMM), ultrasound wave and magnetic field are combined to produce Lorentz Force interaction in tissue to access tissue conductivity. Biological tissue is a conductive element due to the presence of random charges that support cell metabolism. Propagation of ultrasound wave inside the breast tissue will cause the charges to move at high velocity due to the back and forth motion of the wave. Moving charges in the present of magnetic field will experience Lorentz Force. Lorentz Force separates the positive and negative charges, producing an externally detectable voltage that can be collected using skin electrodes. Simultaneously, the ultrasound wave that is initially used to stimulate tissue ionic motion is sensed back by the ultrasound receiver for tissue acoustic evaluation.

A series of experiment and quantification on the output of HMM to breast tissue mimicking phantoms and real breast tissue samples harvested from laboratory mice show that the combination of acoustic and bioelectric properties is a promising way of breast cancer diagnostic. The result shows that acoustic attenuation is lowest for breast tissue mimicking phantom (0.392 ± 0.405 $dBmm^{-1}$). Normal breast tissues experience the highest attenuation (2.329 ± 1.103 $dBmm^{-1}$), followed by cancerous tissue (1.76 ± 1.08 $dBmm^{-1}$) with the difference of 0.569 ± 0.023dB. In addition to that, mean

magnetoacoustic voltage results for tissue mimicking gels, normal tissue and cancerous tissue group are 0.56±0.21 μV, 0.42±0.16 μV and 0.8±0.21 μV respectively.

The experimental data was then fed to an artificial neural network for classification. The network was trained using the steepest descent with momentum back propagation algorithm with *Logsig* and *Purelin* transfer functions. The measurement of ANN performance was observed by using the Mean-Squared Error (MSE) and total prediction accuracy of the network to the testing data. The classification performance of the ANN for testing and validation data is 90.94% and 90%. The classification result shows the advantages of HMM in providing additional bioelectric parameter of tissue instead of only acoustic properties for breast cancer diagnosis consideration. The system's high percentage of accuracy shows that the output of HMM is very useful in assisting diagnosis. This additional capability is hoped to improve the existing breast oncology diagnosis.

ABSTRAK

Penyakit barah payudara merupakan penyakit barah yang paling banyak dihidapi oleh wanita dan merupakan penyebab kematian wanita tertinggi di dunia. Jumlah pesakit barah payudara telah meningkat dengan pengesanan sejuta kes baru yang dilaporkan setiap tahun. Secara purata 373000 kematian turut dilaporkan setiap tahun disebabkan oleh barah payudara. Di Malaysia, laporan Pendaftar Kanser Nasional menyatakan, kadar insiden barah payudara oleh warganegara Malaysia berdasarkan populasi kaum adalah 47.4 bagi setiap 100000 populasi dengan kaum cina mempunyai kadar tertinggi pada 59.9, diikuti kaum india pada 54.2 dan Melayu pada 34.9 bagi setiap 100000 populasi. Dengan peningkatan kadar insiden setiap tahun, penambahbaikan dari aspek diagnosis dan rawatan kanser payudara adalah penting bagi meningkatkan kadar survival.

Dari aspek pengesanan barah payudara, modaliti ultrabunyi digunakan bagi memperoleh penemuan yang lebih spesifik selepas pengesanan dengan menggunakan mammografi adalah meragukan. Ia juga digunakan bagi mengurangkan jumlah prosedur biopsi ke atas pesakit. Walaubagaimanapun, ultrabunyi adalah kurang sensitif dalam mengesan barah payudara. Ini mengehadkan fungsi ultrabunyi sebagai modaliti pengimejan yang digunakan hanya untuk pengesanan sis dan sebagai alat untuk memanduarah proses biopsi. Kajian turut menunjukkan bahawa diagnosis barah payudara melalui ultrabunyi hanya disarankan kepada 40% pesakit yang mempunyai masalah payudara. Ini menunjukkan, sebanyak 60% pesakit yang dirujuk kerana masalah ketumbuhan di payudara tidak disarankan menggunakan ultrabunyi. Situasi ini jelas menunjukkan kekurangan modaliti ultrabunyi yang mengehadkan fungsinya untuk

mengesan barah payudara. Oleh yang demikian, inovasi ke atas pengimejan ultrabunyi adalah amat penting bagi membolehkan modaliti ini mengeksploitasi ciri-ciri tisu yang lain dan menambahbaik proses diagnostik barah payudara yang sedia ada.

Oleh yang demikian, kaedah pengimejan hibrid magnetoakustik telah dibangunkan di dalam kajian ini. Matlamat kepada pembangunan modaliti ini adalah untuk mencipta platform pengimejan yang mampu mengakses ciri-ciri akustik dan bioelektrik tisu. Di dalam kaedah ini, interaksi di antara gelombang ultrabunyi dan medan magnet menghasilkan daya Lorentz yang digunakan bagi mengukur pengaliran elektrik di dalam tisu. Tisu biologi merupakan bahan pengalir elektrik disebabkan kewujudan partikel ion di dalam sel. Pergerakan gelombang ultrabunyi di dalam tisu menyebabkan partikel ion di dalam tisu turut bergerak. Pergerakan ion di dalam medan magnet menghasilkan daya Lorentz yang memisahkan ion positif dan negatif bagi membolehkan pengukuran voltan dilakukan. Selain itu, gelombang ultrabunyi yang pada mulanya digunakan bagi menggerakkan partikel ion di dalam tisu digera semula bagi membolehkan ciri-ciri akustik tisu diukur.

Keputusan pengukuran keluaran ultrabunyi dan voltan HMM ke atas tisu tiruan dan sampel tisu payudara yang diambil daripada tikus makmal menunjukkan gabungan ciri-ciri akustik dan bioelektrik merupakan satu kaedah yang berpotensi tinggi bagi mengesan barah payudara. Kadar redaman ultrabunyi didapati paling rendah pada tisu tiruan (0.392 ± 0.405 $dBmm^{-1}$). Ujian ke atas tisu sebenar menunjukkan kadar redaman paling tinggi berlaku pada tisu normal (2.329 ± 1.103 $dBmm^{-}1$) berbanding tisu kanser (1.76 ± 1.08 $dBmm^{-}1$) dengan perbezaan sebanyak 0.569 ± 0.023dB. Selain itu, keputusan

voltan megnetoakustik pada tisu tiruan, tisu normal dan tisu kanser menunjukkan bacaan min 0.56±0.21 μV, 0.42±0.16 μV dan 0.8±0.21 μV setiap satunya.

Seterusnya, keputusan bagi eksperimen tersebut telah digunakan sebagai input dalam pembinaan rangkaian neural (artificial neural netwok) yang dilatih menggunakan algorithm *steepest descent back propagation with momentum*. Prestasi rangkain neural tersebut diukur melalui nilai *mean squared error* (*MSE)* dan ketepatannya di dalam klasifikasi data ujian dan data validasi. Keputusan klasifikasi menunjukkan ketepatan rangkaian neural tersebut adalah 90.94% bagi data ujian dan 90% bagi data validasi. Peratus ketepatan yang tinggi itu menunjukkan keluaran HMM adalah sangat berguna bagi membantu proses diagnosis onkologi. Kemampuan tambahan ini diharapkan dapat memperbaiki kaedah diagnosis bayah payudara yang sedia ada.

TABLE OF CONTENT

LIST OF TABLES

LIST OF FIGURES

LIST OF SYMBOLS

Y	-	Tissue Admittance
G	-	Tissue Conductance
C	-	Capacitance
ω	-	Angular Frequency
σ^*	-	Admittivity
σ	-	Conductivity
ε_0	-	Dielectric constant of free space
ε'	-	Tissue permittivity
B_0	-	Magnetic field intensity
V_0	-	Particle Velocity
F	-	Lorentz Force
E_0	-	Electric field
J_0	-	Current distribution
W	-	Beam width
I	-	Current
Rc	-	Circuit resistance
D	-	Duty cycle
P_0	-	Peak ultrasound pressure
d	-	Element diameter
Sf	-	Normalized focal length
q	-	Charge
I_c	-	Acoustic intensity
I_f	-	Final acoustic intensity at tissue surface

CHAPTER 1 - INTRODUCTION

1.1 OVERVIEW

Breast cancer is the most common cancer in woman worldwide [15, 101]. In the west, earlier research has demonstrated that 1 in 9 women will develop breast cancer in their life and this risk has been further stratified according to age, with patient up to 25 years, 1 in 15000; up to age 30, 1 in 1900 and up to 40, 1 in 200 [15, 101]. In the South East Asian region, the incident of breast cancer has escalated over the past 20 years especially in Philippine, Malaysia and Singapore [16, 102-103]. With the westernization of Asian countries, changes in reproductive factors, lifestyle and environmental exposures have been proposed to explain the trend [16].

Breast cancer is a disease of uncontrolled breast cells growth, in which the cells acquire genetic alteration that allows them to proliferate outside the context of normal tissue development [6]. In the cancerous tissue, changes in density occur due to uncontrolled cell growth [6, 25, 29] excessive accumulation of protein in stroma [28, 36-37] and enhancement of capillary density [30, 41-43]. On the other hand, changes in conductivity also occur due to increase cellular water and electrolyte content as well as altered membrane permeability and blood perfusion to support metabolism requirements [19, 28, 36-37].

In the current medical practice, ultrasonography plays an important role as an adjunct modality to mammography [45-47]. In addition to that, ultrasonography is also superior to mammography due to its non-ionizing radiations [53]. It is a reliable

modality for solid and cystic benign differentiations with up to 99% reported sensitivity [45, 55-56]. Other than that, ultrasound is used for pregnant and lactating mothers as well as for patient with augmented and inflamed breast [45]. However, the usage of ultrasound in oncology diagnostic is limited by its low sensitivity in detecting small and pre invasive breast cancers [53-55, 57-60] from normal tissues due to the overlapping ultrasonic characteristics of these tissues [33, 92-93]. It is also less sensitive to microcalcification, an important early indicator for certain breast cancer [104]. Furthermore, ultrasound is operator dependant. This means that, a single sonographic image may be interpreted differently by different operators and the result is relative to the operator skills and experience, variations in human perceptions of the images, differences in features used in diagnosis and lack of quantitative measures used for image analysis [55]. This fact has further complicates breast cancer diagnosis via sonography.

Due to the limited capability of ultrasonography, it is very crucial to develop an alternative approach that is capable to manipulate additional breast tissue properties for a better diagnostic result. One of the alternatives is by manipulating bioelectric properties of tissue as an addition to the existing acoustic information given by sonography. Therefore, this expansion of study on the development of novel imaging method for breast cancer detection will concentrate on innovating a new hybrid method that is capable to manipulate the acoustic and bioelectric properties of breast tissue.

1.2 PROBLEM STATEMENT

In the world of oncology diagnostic imaging, the role of ultrasonography is limited by its low sensitivity in detecting small and preinvasive breast cancer from normal tissue due to the similarity in acoustic characteristics between the tissues. This restriction prevents ultrasonography from taking a prominent role in breast screening. Hence, innovation to ultrasound imaging is very crucial so that this modality is capable to explore and manipulate additional properties of breast cancer for better discrimination result.

1.3 OBJECTIVES

1. To develop a new method for tissue imaging that employs the concept of acoustic and magnetism.
2. To study and predict the system output via mathematical calculation
3. To study the effectiveness of the newly developed system for tissue imaging through a series of phantom and animal experiments.
4. To classify the experimental result by using Artificial Neural Network for breast cancer discrimination.

1.4 SCOPE OF WORK

This research is conducted to develop a hybrid imaging method that employs the theory of acoustic and magnetism for tissue imaging by using 9.8MHz ultrasound wave and 0.25T magnetic field. A series of experiment and quantification on the system output to phantom and real biological tissues are also carried out to evaluate the potential of the system. The outcome of the experiment is fed to artificial neural network for performance measurements.

CHAPTER 2 – LITERATURE STUDY

2.1 Introduction

This chapter discussed literature review on various field related to the study particularly in the anatomy of normal and cancerous breast tissue as well as on breast cancer detection. Section 2.2 reviews on the anatomy of normal breast followed by a review on breast cancer in section 2.3. Section 2.4 and 2.5 discussed on bioelectric and acoustic properties of normal and cancerous breast tissue. Section 2.6 and 2.7 review the current ultrasound and magnetoacoustic imaging as modalities for breast cancer detection. Section 2.8 discussed the theory of Hybrid Magnetoacoustic method. Later, section 2.9 looks into the use of artificial neural network in clinical application and its performance measurement. Finally, section 2.10 concludes the review.

2.2 Anatomy of a Normal Breast

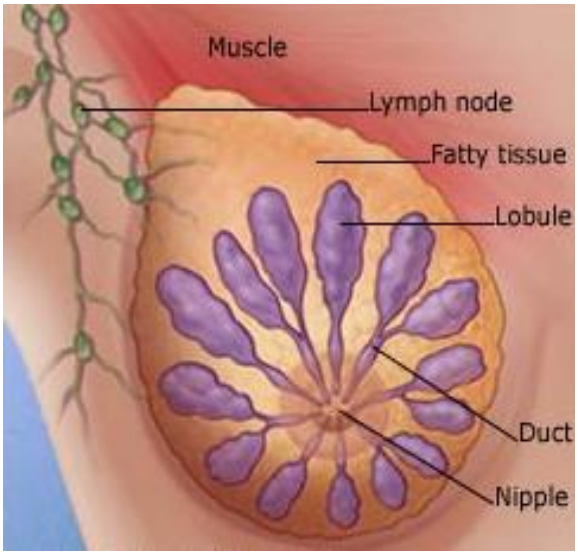

Figure 2.1: Anatomy of the breast [5].

Human breast is a cutaneous organ that produces life sustaining milk for the young. Vertically, it lies between the 2^{nd} and the 6^{th} ribs and horizontally, between the sternal edge and the mid axillary line [2]. The breast is attached to the dermis by fibrous band called coopers ligament on the pectoralis major muscle [18]. Arterial blood supply of the breast is derived from the axillary, intercostals and internal mammary arteries whilst venous drainage is into the axillary and internal mammary veins [2]. The breast also has lymph node, a small gland belongs to the lymphatic system that travels throughout the body as part of the immune system [1-5].

The breast is divided into 15 to 20 glandular units or lobes, with each lobe has a ductal orifice at the apex of the nipple. The stroma within the lobe is specialized containing fine collagen fibers, abundant reticulin and numerous small vessels [2]. The lobes hold microscopic sac called the lobular unit that linked to each other by tiny tubes called ducts. Lobular unit is the most biologically active component of the breast [1-3]. Each breast is estimated to have 10^4 to 10^5 of lobular unit [1]. The epithelial lining of the lobular unit consists of superficial luminal A cells which involve in milk synthesis. In breast feeding, ducts carry milk from the lobular unit towards the areola. At the areola, a few ducts joined together to form a larger duct that ends at nipple. The areolar region, including nipple consists of keratinizing stratified squamous epithelium with a dense basal melanin deposition which accounts for the regions' dark pigmentation. The nipple has multiple lactiferous ducts that range from 2 to 4 mm in diameter.

The volume of the breast varies widely between individuals. Previous study shows that the volume is in the range of 21.1 to 1932 ml with an average of 405.1ml [3]. Breast volume also fluctuates by 0 to 36% following the menstrual cycle [4]. The volume is least during the day 6 to 15 and increasing from the day 16 to 28 by the increasing of parenchymal volume and rising of water content. However, this volume changes are smaller in woman who is taking contraceptive as compared to woman who is not following any family planning regime [4].

Breast development and function depends on estrogen and progesterone hormone which are produced by the ovaries. Prior to puberty, the breast consists of a complex system of ductal structure. At puberty, the gland enlarges when the amount of fibrofatty

elements increase, ducts elongate and small alveolar forms. However, full maturity is only achieved during pregnancy [1]. Finally, postmenopausal breast involution in elderly occurred by regression of the glandular unit with an increase in fat deposition and relative predominance of fibroconnective tissue [2]. At the end stage, only small island of lobules remains with fibrous tissue.

2.3 Breast Cancer

The incidence of breast cancer is increasing over the years with more than 1 million new cases reported each year [15]. Breast cancer accounts for approximately 25% of all female malignancies with a higher prevalence in develop countries [15]. In Malaysia, cancer incidence has escalated over the past 20 years and with the westernization of the Asian countries, it is expected that this trend will continue [16]. Changes in reproductive factors, lifestyle and environmental exposures have been proposed to explain the trend [16].

Breast cancer is a disease of uncontrolled breast cells growth, in which the cells acquire genetic alteration that allows them to multiply and grow outside the context of normal tissue development [6]. The cell metabolism increases to meet the requirements of rapid cell proliferation, autonomous cell growth and cell survival [6]. The term breast cancer describes cancer that is confined in the breast and cancer that has spread out from the breast to another organ. Cancer that metastasizes or spread to other organs is the same disease and has the same name as the primary cancer [2].

The key aspect in diagnosis of breast cancer is to determine whether the cancer is in situ or invasive. In situ cancers confine themselves to the ducts or lobules and do not spread to the surrounding organ. Two main types of in situ breast cancer are the ductal carcinoma in situ (DCIS) and lobular carcinoma in situ (LCIS). DCIS means the abnormal cancer cells are found only at the lining of the ducts. However, it can be found in more than one place in the breast since the cancer travels through the ducts. DCIS has

a high cure rate especially if given early treatments. However, it can change to invasive carcinoma without a proper treatment. LCIS means that the abnormal cancer cells are found in the lining of milk lobules, and is a warning sign of increased risk of developing invasive cancers. Invasive cancer is cancer that has break through normal tissue barriers and invade to the surrounding organs via the bloodstream and the lymphatic system. The most common invasive cancers are invasive lobular carcinoma and invasive ductal carcinoma. There are also some rare cancers such as inflammatory breast cancer and Paget's disease that differ from invasive ductal and lobular carcinoma, in that they do not form a distinct mass or lump in the breast.

The most common symptom of breast cancer is the presence of painless and slowly growth lump that may alter the contour or size of the breast [14, 19]. It is also characterized by skin changes, inverted nipple and bloodstained nipple discharge [14, 19]. The lymphatic nodes under the armpit may be swollen if affected by cancer. In late stage, the growth may ulcerate through the skin and infected [14, 19]. Bone pain, tenderness over the liver, headaches, shortness of breath and chronic cough may be an indication of the cancer spreading to other organs in the body [14].

The main risk factor for breast cancer can be usefully grouped into four major categories [7]: family history or genetics, hormonal, proliferative breast benign pathology and mammographic density. These four factors have now been thoroughly studied and accurate quantitative estimates are available for the factors [7]. In terms of genetics, the mutations of BRCA1 and BRCA2 genes have been identified as genetic susceptibility of breast cancer [7] in which carriers of the genes have at least 40 to 85% chances of getting breast cancer [14]. In this case, gene testing can separate carriers from non carriers at a young age and intervention can be given to those who are positive as early preventive measures [7]. Besides that, several line of evidence points to estrogen levels as a hormonal prime factor for the development of breast cancer [7]. This includes laboratory studies, direct measurement to postmenopausal women [8] and risk reduction when women are taking anti estrogen [9]. However, details of mechanisms are still unclear. In addition to that, risk of cancer following benign breast disease has also been identified. Recent study shows that benign breast disease in the absence of proliferation does not carry any excess risk [7]. However, simple hyperplasia doubles the excess rate

and atypical hyperplasia increase the risk of getting breast cancer to 4 fold [7, 10]. In terms of mammographic density, earlier studies have clearly demonstrated that a radiographically opaque area in the mammography is an important measure of the risk of developing breast cancer [7, 11-12].

Finally, female breast has a special place in human affairs beyond its biologic function. It was a prominent feature of motherhood, beautifulness, fertility and abundance since the early days. Disease of the breast particularly cancer is not only a threats to women health and well being but are also attacks on femininity, nurturance, motherhood and personal identity. Hence, efforts to improve breast cancer detection and treatment must continue not only to save lives but also as part of the social betterment.

2.4 Bioelectric Property of Normal and Cancerous Breast Tissue

Bioelectric property of tissues in the human body differs significantly depending on their structures [19]. Human tissue consists of cellular structure surrounded by a resistive extracellular fluid that contains water and electrolytes. On the other hand, the cell membrane composed of lipid bilayer and ion channel that is capacitive and resistive. Hence, the serial representation of tissue bioelectric properties is described by:

$$Y = G + J\omega C$$

where Y =1/Z is admittance, G is the conductance, C is the capacitance and ω is the angular frequency. Admittance is also represented by admittivity which is expressed as

$$\sigma^* = \sigma + j\omega\varepsilon_0\varepsilon'$$

Where σ^* is tissue admittivity, σ is tissue conductivity, ε' is tissue permittivity and ε_0 is the dielectric constant of free space. Bioelectric properties of tissue also vary with the

frequency of the applied electric field following α, β and γ dispersion [19- 20]. The α dispersion occurs at low frequency (10Hz to 10 kHz) and is caused by the ionic environment that surrounds the cell. The β dispersion is a structure relaxation in the frequency of 10Hz to 10MHz. At higher frequency, the γ dispersion is found related to water molecules. The α and β dispersion regions are more interesting in medical application since most changes between normal and cancerous states occur in this range [19, 21].

Bioelectric measurement for human breast tissue has started since 1920's with the measurement of excised normal and cancerous breast tissues. Compared to normal tissue, malignant tissue has higher conductivity [22-23] and permittivity [22-25] and lower impedivity [26-27]. These changes are due to the increase cellular water and electrolyte content as well as altered membrane permeability and blood perfusion [19, 28, 36-37]. Study by [23] in the frequency range of 3MHz to 3GHz shown that conductivity, σ and permittivity, ε of malignant tissue are higher than normal tissue particularly at frequencies below 100MHz. The research reveals that, σ is from 1.5-3mS/cm for normal tissue and from 7.5-12mS/cm for malignant tissue, whilst ε is about 10 for normal tissue and 50-400 for malignant tissue. At the frequency of 20kHz to 100MHz, comparative bioelectric study [22] between tumor and its peripheral tissue shows that cancerous tissue has higher conductivity, σ and permittivity, ε than the surrounding tissue. Data from a few tumor samples indicates that σ ranges from 0.3-0.4 mS/cm for normal, from 2.0 to 8.0 from cental part of tumor, ε ranges from 8-800 for normal and 80 to above 10000 for central part of tumor. At the frequency of 0.488 kHz to 1MHz, the impedivity modulus for cancerous tissue is (243±77 to 245±70Ωcm), and is lower than its surrounding adipose fatty tissue (1747±283 to 2188±338 Ωcm) and connective tissue (859±306 to 1109±371 Ωcm). At frequency above 100kHz, cancerous tissue exhibit the most capacitive response of all group [25] while another study found that complex conductivity and characteristics frequency are largest for cancerous tissue, middle for transitory tissue and lowest for normal tissue [117].

From these measurements, it can be observed that bioelectric parameters are expressed in various electric term. However, the common conclusion that can be drawn

is there are significant differences in bioelectric properties between normal and malignant tissue.

2.5 Density of Normal and Cancerous Breast Tissue

The mammary gland is a complex tissue that consists of epithelial parenchyma embedded in an array of stromal cell [28]. It undergoes dynamic changes over the lifetime of a woman from the expanded development at puberty, to proliferation and apoptosis during the menstrual cycle and to full lobuloalveolar development for lactation. Breast carcinoma is a disease of uncontrolled cell growth in which mutated cells acquire genetic alteration that allow them to proliferate, grow and pile up outside the context of normal tissue development, which finally result in increased local cell density [6]. In addition to that, it is well established that stroma associated with normal mammary gland development is totally different from that associated with carcinoma [28, 36]. Compared to normal breast tissue, the stroma accompanying breast carcinoma contains increased protein, immune cell infiltrates and enhanced capillary density [28, 36, 37]. Extensive multi proteins accumulation in the stroma has also been associated with enhanced growth and invasiveness of the carcinoma [30]. Increased collagen 1 and fibrin deposition, elevated expression of alpha smooth muscle actin (αSMA), collagen IV, prolyl-4-hydroxilase, fibroblast activated protein (FAP), tenascin, desmin, calponin, caldesmon and others have collectively altered the structure, stiffness and density of the extracellular fluid [28, 36-40]. Enhanced capillary density or angiogenesis is the complex process, leading to the formation of new blood vessels from the preexisting vascular network and further increased the compactness of tissue [34]. The formation of angiogenesis is induced by the secretion of specific endothelial cell growth factors produced by the tumor or the stromal cells [34]. Studies show that angiogenesis plays an important role in facilitates further tumor progression [30, 41-43].

In oncology research works, a few methods were used in estimating densities of normal and cancerous breast tissues. This includes cellular content estimation by

monitoring the level of certain cell parameters that are elevated or reduced in proportion to tissue density, or via image estimation by monitoring imaging parameter that change following changes in tissue density.

In cellular content estimation, studies show that the elevation and reduction of p73 gene [29] and matrix metalloproteinases (MMPs) [35] level is associated with tissue density. p73 is a member of the p53 family of transcriptions factors with 2 isoforms of α and β that is implicated in cell differentiations and development. Observation found that the level of p73α increases with increased cell density whilst p73β decreases with increased cell density. Over and under expression of this protein's isoforms in breast cancer are used to confirm an altered cellular density in breast carcinoma. On the other hand, MMPs are a large family of metal-dependent matrix degrading endopeptidases implicated in numerous aspects of tumor progression [35, 44]. Recent studies revealed that the expression of MMPs is elevated in an aggressively growing and densely packed breast cancer cell line [35].

In medical imaging, changes in breast density due to carcinoma are usually assessed by using mammography and ultrasound. Mammographic density refers to the relative abundance of low density adipose tissue to high density glandular and fibroblastic stromal tissue within the breast. Previous study shows that, the involvement of 60% or more of the breast with mammographically dense tissue confers 3 to 5 fold increased risk of breast cancer [28]. In ultrasonography, changes in tissue density are indicated by the changes in velocity. Ultrasound velocity increases when it travels through a dense material and decreases when it travels through a less dense material [32]. This study report is in agreement with earlier observation that shows ultrasound velocity travelling through breast carcinoma is higher than those of normal tissue [33].

The presented literature supports the fact of density alteration in breast carcinoma. In general, the density of mammary fat pad is 928kg/m3 and 1020kg/m3 for normal tissue. However, due to the altered density of breast carcinoma, research in [31, 125-126] estimates the density of breast carcinoma to be very close to muscle which is 1041kg/m3 [31].

2.6 Ultrasonography in Breast Oncology Diagnostic

Breast ultrasonography means imaging the breast with ultrasound [18]. It is an interactive imaging process by using sound wave at the frequency of 20kHz to 200MHz [18]. In the world of medical diagnostic, breast ultrasonography has an established and significant role in diagnostic of breast abnormalities [45]. Ultrasound is superior from mammography for its non-ionizing radiation. This makes ultrasound an imaging of choice to manage symptomatic breast in younger women as well as in pregnant and lactating mother whom the theoretical radiation of mammography is pertinent [53]. Ultrasonography is also a reliable modality for solid and cystic breast anomaly differentiation [45-47, 55-57, 60]. It is also used in imaging augmented and inflamed breast. However, in the current practice, the proportion of patient in whom breast ultrasonography is considered necessary is only 40% [60]. This means that, ultrasonography is not indicated for the rest 60% of patients referred for breast imaging [60]. This practice explains major constraint of ultrasonography in breast imaging that limits its usage for diagnostic of breast symptoms and for screening asymptomatic patients [53-55, 57-60].

The major problem of ultrasonography is its low sensitivity in detecting small and preinvasive breast cancers [53-55, 57-60] from normal tissues due to the overlapping ultrasonic characteristics in these tissues [92-93, 127]. Breast ultrasound diagnostic relies on several sonographic features that are based on margin, shape and echotecture. Breast cancers are often characterized by poorly defined margins, irregular borders, spiculation, marked hyperechogenicity, shadowing and duct extension [56].

A systematic review on 22 independent studies to investigate the sensitivity of ultrasound in breast cancer detection was conducted by Flobbe *et al* in [60]. In the review, patient population was divided into 4 groups namely: 1. Patient undergoes clinical examination and mammography. Hence, ultrasound interpretation is with the knowledge to prior mammography (5 studies), 2. Patient undergoes mammography and clinical examinations. Hence, interpretation is based on the previous clinical and imaging data (4 studies), 3. Patients are referred for pathology and mammography. Hence, ultrasound interpretation is with the knowledge to prior mammography result (6

studies) and finally, 4. Ultrasound is interpreted blindly without prior patient clinical data (7 studies). Average ultrasound sensitivity for each group of patient is: 82.6%, 88.25%, 86.83% and 82.57 respectively. This systematic review has revealed the weakness of ultrasound in diagnostics of patients with breast abnormalities regardless the existing of prior patient clinical examination and mammography. The study concludes that little evidence support was found to confirm the well recognized value of ultrasonography in breast cancer detection. Other than the review, independent report by [110] also shows the low sensitivity of ultrasound in detection of breast cancer.

Another limitation of ultrasound is its inability to detect microcalcification, a calcium residue found in the breast tissue as an early indicator of DCIS [55]. In ultrasonography, the presence of microcalcification in tissue is often masked with breast tissue heterogeneity and grainy noise due to speckle phenomena [111-112]. The reasons make microcalcification detection with ultrasonography unreliable [55].

In addition to that, study in [59] reported the sensitivity of ultrasonography for breast cancer detection evaluated by 3 different radiologists with experienced from 8 to 16 years. The result shows that the achieved sensitivity is 66.7%, 87.5% and 56.3% for the three radiologists. This study found that, breast ultrasound diagnosis is not only complicates by the low sensitivity of the ultrasound itself but also by the dependency of ultrasound result to operator. This means that, a single sonographic image may be interpreted differently by different operators and the result is relative to the operator skills and experience, variations in human perceptions of the images, differences in features used in diagnosis and lack of quantitative measures used for image analysis [55].

This inter-reader variability has led to automated ultrasonographic image evaluation via Computer Aided Diagnosis (CAD System). CAD is a multi step process that involves identification of lesion by segmentation, extraction and recognition by using a complex and intelligent algorithm based on echo texture, margin and shape [55]. It offers potentially accurate judgment to generate valuable second opinion in assisting diagnosis [55]. In CAD, the area under the ROC curve is the performance metric to evaluate CAD with 1 represents perfect performance [55]. Studies have shown that sonographic CAD is able to give a good classification performance of 0.83-0.87 [105-

106, 108], excellent performance of 0.92 [107] and near perfect performance 0f 0.95-0.98 [109]. With the increasing acceptance of Mammo CAD and MRI CAD, Sonographic CAD has also widely accepted to assist in diagnostics. In addition to that, [61-62] also proves that sonographic CAD is helpful for diagnosis.

Although breast ultrasound diagnosis has improved over the time with the usage of CAD, its usage in breast cancer detection is still limited due to its low detection sensitivity to breast masses and microcalcification as well as inter-reader variability. Hence, additional tissue properties need to be further explored for better breast cancer detection method.

2.7 Lorentz Force Based - Magnetoacoustic Imaging

Research in Lorentz Force based magnetoacoustic imaging had started since 1998 when Wen *et al* [63-65] developed a 2D Hall Effect imaging (HEI). HEI combines the theory of acoustic and magnetism, to manipulate the resulting voltage that rises from the interaction between the two energies for bioelectric profiles measurement. In HEI, non-focused ultrasound wave and magnetic field are combined to produce Lorentz Force interaction in tissue to access tissue conductivity [63-65]. Biological tissue is a conductive element due to the presence of random charges that support cell metabolism [65]. Propagation of ultrasound wave inside the breast tissue will cause the charges to move at high velocity due to the back and forth motion of the wave [63-65]. Moving charges in the present of magnetic field will experience Lorentz Force. Lorentz Force separates the positive and negative charges, producing an externally detectable voltage [3-8] that can be collected using a couple of skin electrodes [63-68]. HEI was first tested to image a phantom made of polycarbonate that is immersed in saline solution. Later, it was tested to image biological tissue. A series of experimental studies on HEI shows that, the resulting voltage that is collected is linearly proportional to the magnetic field strength and the ultrasound-induced velocity of the ionic particle.

Later, study in [66] used HEI experimental set up to measure current output from agar samples prepared from 10g/l NaCl saline and 2.5% of agar powder. This research indicates that HEI is a new modality with high potential to measure electric conductivity of biological media by using ultrasound as probe. In addition to that, study in [67] improves HEI's set up when a focused ultrasound transducer is used to focus the sound wave at a focal point. This was to prevent high attenuation from occurred in tissue through beam localization. Beam localization minimizes Lorentz Force interaction to only the focus area to maximize the interaction effects and increase the resulting voltage value. Therefore, the ultrasound probe was attached to a 1mm step size motor so that scanning can be done by moving the focused transducer and 2D image can be generated. As a result, better voltage/current value was obtained for profile assessment of tissue.

Based on the review, previous magnetoacoustic imaging manipulates Lorentz Force interaction for only bioelectric profile assessment of tissue. The output of ultrasound wave that is initially used to stimulate tissue particle motion is ignored, though it contains valuable information with regards to tissue mechanical properties. Hence, this study employs the concept of magnetoacoustic imaging with acoustic and bioelectric outputs to improve the existing breast cancer detection method.

2.8 Theory of Lorentz Force Based - Magnetoacoustic Imaging

Theoretically, magnetoacoustic imaging manipulates the interaction between ultrasound wave and magnetic field in current carrying media. Consider an ion in a biological tissue sample with charge q and conductivity σ. The longitudinal motion of an ultrasound wave in z direction will cause the ion to oscillate back and forth in the medium with velocity $\mathbf{V_0}$. In the presence of constant magnetic field $\mathbf{B_0}$ in y direction, the ion is subjected to the Lorentz Force [63-68]:

$$\mathbf{F} = q[\, v(z,t) \times \mathbf{B_0} \,] \qquad (1), [63\text{-}68]$$

From (1), the equivalent electric field is :

$$\mathbf{E_0} = \boldsymbol{v}\,(z,t) \text{x } \mathbf{B_0} \qquad (2),\ [63\text{-}68]$$

The field $\mathbf{E_0}$ and current density $\mathbf{J_0}$ oscillate at the ultrasonic frequency in a direction mutually perpendicular to the propagation path (direction of $\mathbf{v_0}$) and the magnetic field $\mathbf{B_0}$. This produces an electric current density given by:

$$\mathbf{J_0} = \sigma[\,\boldsymbol{v}\,(z,t) \text{x } \mathbf{B_0}\,] \qquad (3)\ ,\ [63\text{-}68]$$

The net current *I(t)*, is derived by integrating (3) over the ultrasound beam width, **W** along the propagation path:

$$I(t) = W\boldsymbol{B_0}\int_{Soundpath\ initial}^{Final} \sigma \boldsymbol{v}(z,t)dz \qquad (4)\ ,\ [63\text{-}68]$$

Hence, if current *I(t)* is collected by electrodes into a detection circuits having impedance *Rc*, the detected voltage is:

$$V(t) = R_c W\boldsymbol{B_0}\int_{Soundpath\ initial}^{Final} \sigma \boldsymbol{v}(z,t)dz \qquad (5)\ ,\ [63\text{-}68]$$

Based on the equations, voltage that is proportional to the conductivity weighted density of the tissue can be accessed for evaluation from the x direction. Concurrently, the ultrasound signal that is used to stimulate the ionic motion can be collected for acoustic evaluation from the z direction.

2.9 Artificial Neural Network in Biomedical and Clinical Application

Artificial intelligence has been used very extensively in modeling biomedical application. It has been proposed as reasoning tool to support clinical decision making since the earliest day of computing. An artificial neural network (ANN) is a nonlinear and complex computational mathematical model for information processing with architectures inspired by neuronal organizational biology [69-71]. The underlying reason for using an artificial neural network in preference to other likely methods of solution is its ability to provide a rapid solution. Depending on the type of problem being considered, ANN is a proven method which is a capable of providing fast assessment and accurate result [69-72]. This is because; ANN works in a simulated parallel manner and is not limited by the serial requirements of the normal program such as in expert system and conventional programming [69-72].

The most valuable property of ANN is its ability to learn and to generalize [72]. Generalization refers to the capability of neural network to produce reasonable outputs for input which is not encountered during training [69, 73]. These attributes mark neural network out from other computational methods [72]. Neural network consists of a number of simple and highly connected processors. Like the brain, ANN can recognize pattern, manage data and most significantly, learn [69-70]. Previous study also showed that, ANN with at least one hidden layer of computational unit is capable of approximating any finite function to any degree of accuracy as a universal approximator [74].

In medicine, ANN is widely used for modelling, data analysis and diagnostic classifications [69-71, 74-76]. The most common ANN model used in clinical medicine is the multilayer perceptron (MLP) [75]. The most widely used connection pattern is three layer back propagation neural network which have been proved to be useful in modelling input –output relationship [69-70, 77] while the most commonly used transfer functions are linear, log sigmoid and tan sigmoid [78].

The most commonly used indicator of ANN performance is Mean Squared Error (MSE). MSE is the average of the squares of the difference between each output and the desired output. Research performed in [69-70, 73, 75-76, 78-79] used MSE as the measurement of ANN performance. In addition to that, researches conducted in [73, 79, 80-82] were using the accuracy of the tested data as one of the performance indicator of the ANN. By using this method, network is trained using a part of the data and the remainder is assigned as the testing and validation data.

2.10 Conclusion

The limitation of breast ultrasound in cancer diagnostic is its low sensitivity in detecting small and preinvasive cancer from normal tissue, due to the overlapping acoustic characteristic between those tissues. This restriction prevents ultrasound from taking a prominent role in managing symptomatic patient as well as in breast screening.

However, studies have shown that normal and cancerous breast tissues differ to each other in density and conductivity. The changes in density are due to uncontrolled cell growth, excessive accumulation of protein in stroma and enhancement of capillary density. On the other hand, conductivity changes are due to increase cellular water and electrolyte content as well as altered membrane permeability and blood perfusion to support metabolism requirements. Whilst ultrasound imaging is very sensitive to density, further innovation needs to be done to the modality so that it is capable to explore additional properties of breast tissue for cancer detection.

Hence, a novel hybrid method is developed in this study to evaluate the effectiveness of magnetoacoustic imaging in breast cancer detection.

CHAPTER 3 – METHODOLOGY

3.1 Introduction

This chapter describes the methodology that was employed in this study. The methodology comprises of 6 stages. The first stage began with literature review on the anatomy and physiology of normal and cancerous breast tissue as well as breast cancer detection method. The second stage involved a mathematical calculation on the fundamental physics of HMM to predict the system's output. The fundamental calculation was followed by a series of experiments, to observe the HMM outputs to phantom and biological tissue for breast cancer evaluation (stage three). The experiment comprises of ultrasound attenuation measurement and magnetoacoustic voltage measurement. The experimental database was then statistically quantified to discriminate the attenuation and magnetoacoustic voltage value for normal and cancerous tissue group (stage four). After quantification, the database went through data cleaning and normalization process, to be used in ANN development process (stage five). The final stage was a validation study to the developed artificial neural network. The stages were summarized in the flow chart below:

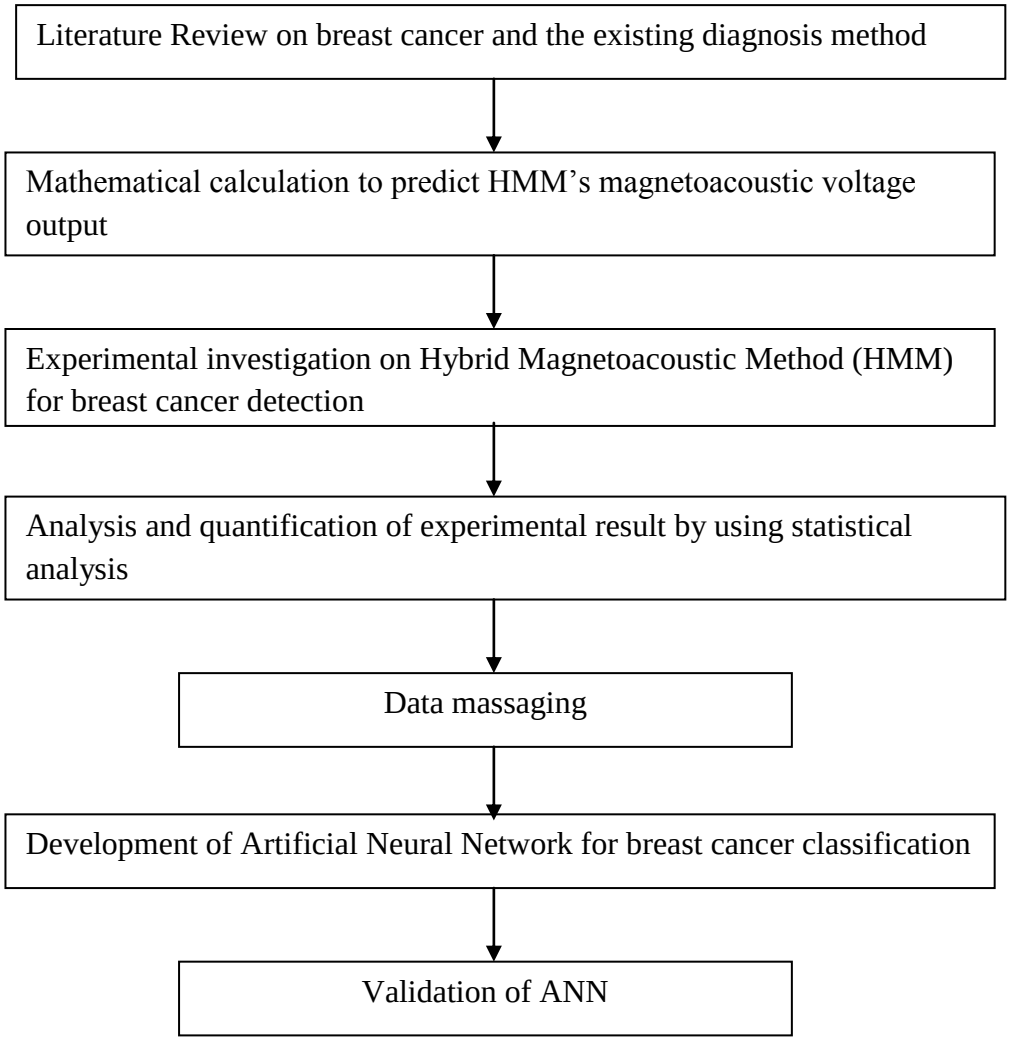

Figure 3.1: Flow chart for the development of HMM for breast cancer detection

3.2 Mathematical Calculation for HMM Voltage Output Prediction.

The objective of this mathematical calculation was to acquire an accurate prediction value of HMM voltage output. The magnetoacoustic voltage output comprises of 2 peaks with the first peak has a positive value and the other peak has a negative value. The 2 peaks represent the boundaries of the scanned object. The voltage calculation involved 5 different steps namely: 1) Modelling of experimental condition, 2) Determination of acoustic power of the ultrasound circuit, 3) Determination of ultrasound intensity, 4) Determination of ultrasound peak pressure and particle motion velocity and finally 5) Determination of Lorentz Force and the resulting magnetoacoustic voltage value.

3.2.1 Modelling of Experimental Condition

Before the calculation was started, modelling of experimental condition was done following the real experimental planning [125-126]. In general, the HMM system consists of a cylindrical permanent magnet, a unit of ultrasound pulser receiver, 2 units of 9.8MHz ultrasound transducer to transmit and receive the ultrasound wave and a couple of skin electrodes for magnetoacoustic voltage output collection.

3.2.1.1 Magnetic Field**.**

A cylindrical permanent magnet was used to produce a static magnetic field with intensity of 0.25T at the center of the magnet bore. The magnet bore has a diameter of 5cm. A measurement chamber was placed at the center of the magnet bore, and the magnitude of the magnetic field intensity was assumed to be homogenous throughout the measurement chamber [125-126]. The magnetic field direction was set in the positive y direction, perpendicular to the ultrasound wave.

3.2.1.2 Ultrasound System

The ultrasound pulser receiver unit delivered 9.8MHz negative pulses with amplitude of 400V to a couple of single element, nonfocused ceramic transducers. The element diameter, D of the transducer is 5mm. The impedance value of the ceramic transducer is 190 Ω at 9.8MHz for a thickness of 150μm to operate at the frequency range of 6.28-14.3 MHz [88]. The ultrasound transducers were permanently attached to the measurement chamber that placed the tissue model. The ultrasound beam direction was set in the z direction.

3.2.1.3 Ultrasound Propagation Path

The ultrasound signal was emitted from the matching layer of the ultrasound transducer in the z direction (direction of the chamber depth). The sound wave will propagate through a 4mm depth of oil layer followed by a 2mm thickness breast tissue samples before sensed back by the receiver transducer.

3.2.2 Determination of Acoustic Power of the Ultrasound Circuit

The ultrasound pulser and receiver unit delivered 400V of 9.8MHz alternating negative voltage pulses to the ultrasound transducer at a Pulse Repetition Frequency (PRF) of 5kHz. In the ultrasound transducer, the voltage pulses produced an electro-mechanical resonant at the piezoelectric element, so that ultrasound waves at 9.8MHz will be emitted. The strength of the resulting ultrasound wave is proportional to the given electric power as the rate of transport of ultrasound energy [86-88]. Hence, the acoustic power of the ultrasound wave was calculated by determining 1) The delivered average voltage, 2) The delivered electric power and finally 3) The delivered acoustic power [86-88].

Average voltage is the mathematical average of all instantaneous wave voltage pulses that occur at each voltage alternation [83]. The average voltage for the wave was calculated following the formula:

$V_{average} = Duty\ Cycle\ x\ Peak\ Voltage$ (6), [83-84]

In which,

$Duty\ cycle, D = \frac{\tau}{T}$ (7), [83-84]

With τ=duration of an active function and T is the period of the function. Mathematically, $\tau = \frac{1}{f}$ and $T = \frac{1}{PRF}$, in which *f* is the signal frequency and PRF= Pulse Repetition Frequency.

When the average voltage was known, the total electric power of the ultrasound system was calculated following the equation:

$P_{electric} = \frac{V_{average}^2}{Z_t}$ (8), [85]

In which, Z_t is the impedance of the piezoelectric ceramic element at 9.8MHz.

Finally, the acoustic power can be calculated by

$P_{acoustic} = P_{electric}\ x\ K_c$ (9), [18, 86-88]

Where K_c , is the electroacoustic coupling constant of the ceramic element.

The acoustic power is a measure of ultrasound energy per unit of time. It is measured in Watts and regarded as ultrasound beam intensity times the beam area [18, 86-87].

3.2.3 Determination of Ultrasound Beam Intensity

Medical ultrasound is produced in the form of ultrasound beam that focuses to certain area and the beam's strength is described in term of beam intensity, defined by power per unit area (W/m^2) [86- 89]. The beam intensity, I_c at the time the ultrasound wave leaves the matching layer of the transducer was determined from the equation:

$$I_c = \frac{P_{acoustic}}{beam\ area} \qquad (10), \quad [18, 86\text{-}89]$$

In which, $Beam\ Area = \pi\left(\frac{beam\ diameter}{2}\right)^2$ and $Beam\ Diameter = 0.2568D\ x\ S_F$ (11), [90]. In which, D = element diameter, S_F = normalized focal length with its value is 1 for a flat transducer [90]. In this study, the element diameter D, for the transducer is $5e^{-3}$ m.

Soon after the ultrasound wave leaves the transducer, it propagated through a 4mm depth of oil and experienced energy loss via attenuation. Previous report [117] on average attenuation of edible oil at 10MHz is 59Np/m in which, equals to 5.12dB/cm. Hence, for a 4mm depth of oil, it was approximated to be very close to 3dB.

Due to the -3dB loss, the remaining ultrasound intensity at the time it hits the tissue surface was 50% of its original intensity. Hence, the attenuated intensity value was:

$$I_f = \frac{50}{100} x\ I_C \quad [18]$$

3.2.4 Determination of Peak Ultrasound Pressure and Particle Motion Velocity.

When the ultrasound beam with intensity of I_f passes a point in the tissue sample, the particles in the tissue were alternately compressed together and pulled apart leading

to oscillation in the local pressure. The peak pressure P_0, during the passage of the pulse was calculated following the equation:

$$P_0 = \sqrt{I_f \, x \, z} \qquad (12), \quad [68, 86\text{-}87, 90],$$

Where z, is the normal and cancerous tissue acoustic impedance of $1.54e^6$ Rayls [86].

However, this initial pressure was the total pressure that creates a longitudinal and shear wave in the breast tissue. Previous study reported that as much as 36% of ultrasound pressure is converted to the form of shear wave especially in highly elastic material such as breast cancer tissue, and the remaining is in the form of longitudinal wave [124]. Since the value of Lorentz Force is only influenced by the longitudinal wave in z direction, the final peak pressure was calculated by considering only the remaining 64% of the initial peak pressure. Hence, the final pressure, P_f was calculated as follows:

$$P_f = \frac{64}{100} x \, P_0 \text{ [124]}$$

From the final peak pressure, the velocity of particle motion was calculated following:

$$V_0 = \frac{P_f}{\rho c_0} \qquad (13), \quad [68]$$

In which, P_f = final ultrasound pressure calculated previously, ρ = breast tissue density, c_0 = speed of sound in the medium.

3.2.5 Determination of Lorentz Force and magnetoacoustic voltage value

Finally, the Lorentz Force and the magnetoacoustic voltage value were calculated following equation [63-68]:

$F = qE$ (1), [63-68]

$E = \mathbf{V_z} x \mathbf{B_y}$ (2), [63-68]

$J_x = \sigma[\mathbf{V_z} x \mathbf{B_y}]$ (3), [63-68]

$I = \int J_x . dS$ (4), [63-68]

The calculation above estimates the value of the first peak of magnetoacoustic voltage signal that occurs at the upper boundary of tissue. The amplitude of the second peak was calculated by further analyzing the attenuation of ultrasound intensity after propagating through the 2mm tissue and finally hit its lower boundary. From there, the peak pressure of ultrasound was recalculated to find the second peak value.

Then, the value of the first positive and the second negative peak was averaged to find the final magnetoacoustic voltage value. Averaging was done to correlate the calculation result with the experimental result since the lock in amplifier that was used in the experimental investigation gives an average output of signal minimum and maximum.

3.3 Experimental Investigation on Hybrid Magnetoacoustic Method (HMM) for Breast Cancer Detection

The experimental investigation comprises of 4 steps including 1) experimental set up, 2) preparation of samples, 3) ultrasound measurement and 4) magnetoacoustic voltage measurement.

3.3.1 Experimental Set Up

The entire experimental study was conducted in an anechoic chamber with shielding effectiveness of 18KHz to 40GHz, located at the Center of Electromagnetic Compatibility, Universiti Tun Hussien Onn Malaysia. Electromagnetic shielded environment was preferred to prevent external electromagnetic interference from contaminating the recorded magnetoacoustic voltage and interrupting the sensitive lock-in amplifier readings. Interior setting of the anechoic chamber at the Center of Electromagnetic Compatibility, UTHM was shown in figure 3.2.

The HMM system consists of a 5077PR Manually Controlled Ultrasound Pulser Receiver unit, Olympus-NDT, Massachussets, USA. The unit delivered 400V negative wave pulses at the frequency of 10MHz and PRF of 5KHz, to 2 units of 0.125 inch standard contact, single element ultrasound transducers having center frequency of 9.8MHz. The transducers were used to transmit and receive ultrasound wave in transmission mode setting from the z direction. The pulser receiver unit was also attached to a digital oscilloscope, model TDS 3014B, Tektronix, Oregon, USA for signal display and storage purposes.

A custom made, 15cm height cylindrical permanent magnet was used to produce static magnetic field, with intensity of 0.25T at the center of its bore. Diameter of the magnet bore is 5cm. The direction of magnetic field was set from the y axis.

Magnetoacoustic voltage measurements were made from the x direction with respect to the measurement chamber. It was conducted by using 2 unit of custom made, ultrasensitive carbon fiber electrodes. The sensitivity of the Carbon Fibre electrodes is

0.1µV. Carbon fiber electrodes have also been used for electrophysiological studies and voltammetric analysis due to its significantly less noise [118-120]. Furthermore, carbon fiber has a very weak paramagnetic property compared to other conventional electrodes. Due to the property, carbon fiber has been used in combination with fMRI to study the brain stimulation [120-122]. The carbon fiber electrodes were connected to a high frequency Lock-In amplifier, model SR844, Stanford Research System, California, USA. The full scale sensitivity of the amplifier is 100nVrms with 80dB dynamic reserve [123]. Figure 3.3 and 3.4 show the measurement chamber and its positioning inside the permanent magnet bore respectively.

Figure 3.2 Anechoic chamber at the Center of Electromagnetic Compatibility, UTHM.

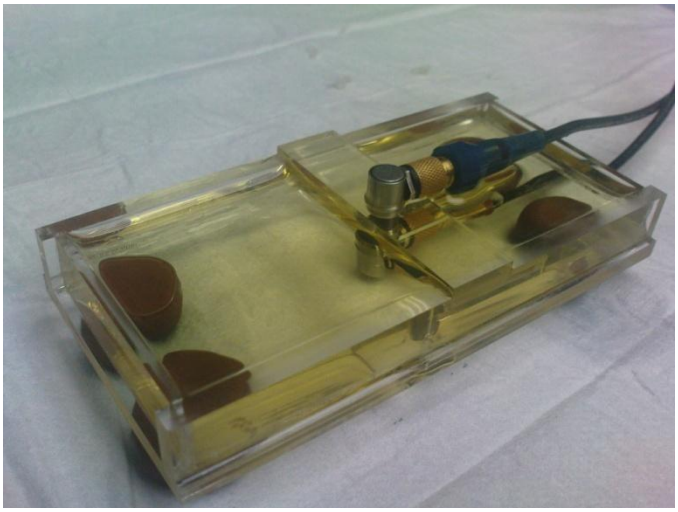

Figure 3.3 Measurement chamber

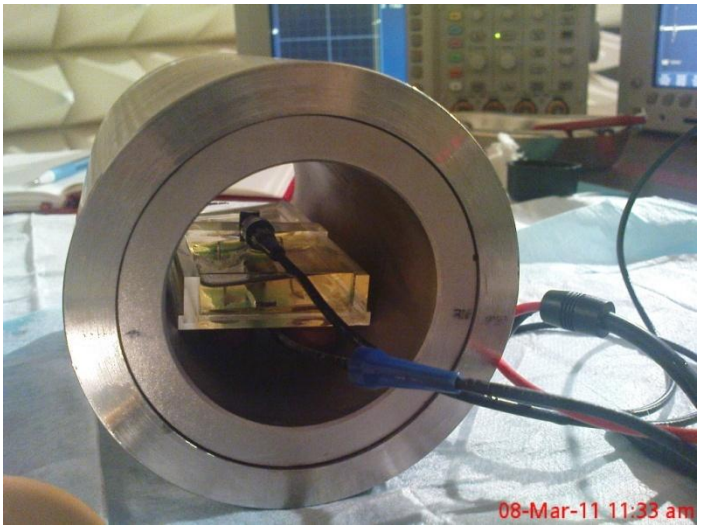

Figure 3.4: Measurement chamber position inside the permanent magnet bore

3.3.2 Preparation of Samples

Two types of samples were used in this study. The first sample was a set of tissue mimicking gel with properties that are very close to normal breast tissue. Another sample was a set of animal breast tissues that was harvested from a group of tumor bearing laboratory mice and its control strain. The tissue mimicking gel was used in the early part of this study to understand the basic response of HMM system to linear

samples before it was tested to complex samples like real tissues. The same experimental planning was also observed in previous studies [63-65, 94-95], in which phantoms were tested to their system before it was tested to real biological tissue.

3.3.2.1 Preparation of Tissue mimicking gel

The tissue mimicking gel was prepared from a mixture of gel powder, sodium chloride (Nacl) and pure water at the right proportion to achieve the desired density and conductivity. During the preparation, 200 ml of pure water was added to 40 ml of agar gel powder. The solution was stirred and 80 ml of NaCl was added to the solution. After that, it was poured into a preparation mold (plastic container in cube shape) for 30 minutes. The density and conductivity of the breast tissue mimicking gel was 1114 Kg/m3 and 0.27S/m respectively.15 samples of breast tissue mimicking gel were used in this study. During the experiment, the samples were cut down to an approximately 1cm x 1cm size with 2mm thickness. Thickness standardization was made by using a U-shaped mold with 2mm opening.

3.3.2.2 Preparation of Real Animal Tissue

The used of animal in this study was approved by the National University of Malaysia Animal Ethics Committee. Transgenic mice strains FVB/N-Tg MMTV PyVT 634 Mul and its control strain FVB/N were obtained from the Jackson Laboratory, USA. For the transgenic mice set, hemizygote male mice were crossed to female noncarrier to produce 50% offspring carrying the PyVT transgene.

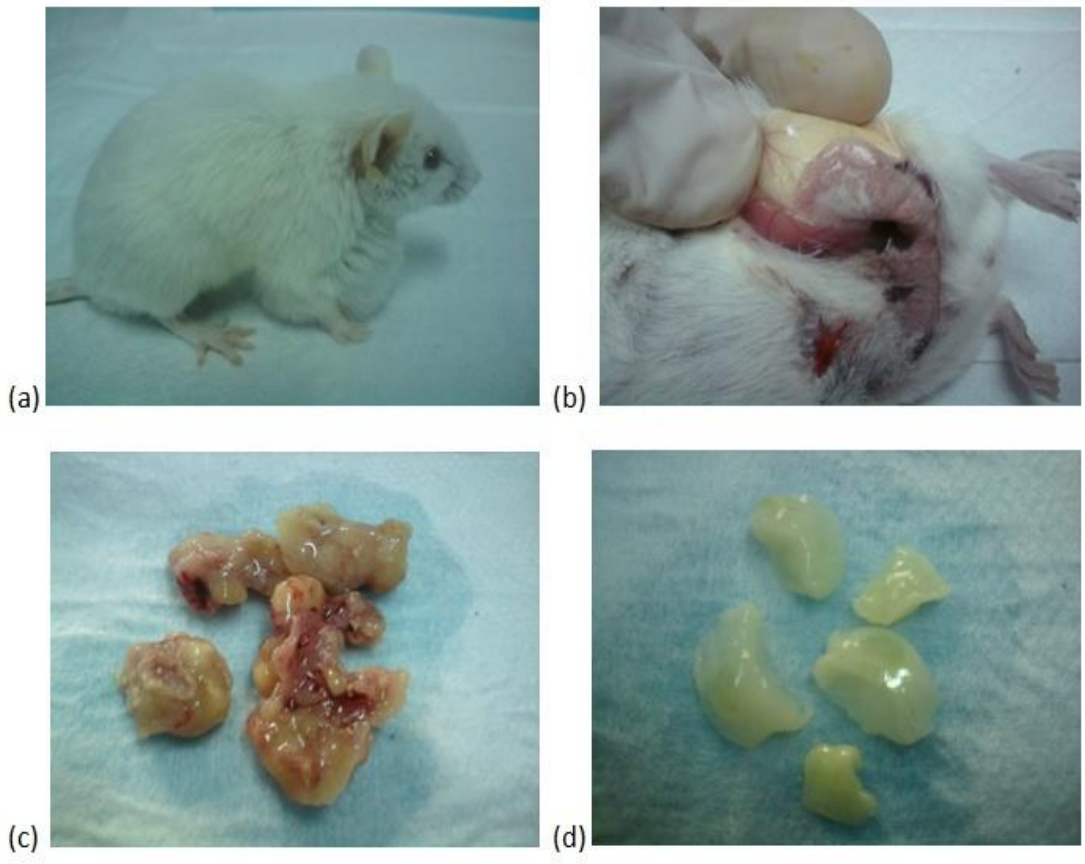

Figure 3.5: Mice breast cancer model that was used in this study. (a) Transgenic mice strain FVB/N Tg-MMTV PyVT that was genetically confirmed to carry invasive breast adenocarcinoma. (b) Surgical process was done to harvest the breast tissues. (c) Cancerous breast tissues. (d) Normal breast tissues.

Transgene expression of the mice strain is characterized by the development of mammary adenocarcinoma in both male and female carriers with 100% penetrance at 40 days of age [114-115]. All female carriers develop palpable mammary tumors as early as 5 weeks of age. Male carriers also develop these tumors with later age of onset [114, 116]. Median age of tumor latency is 66 days in female and 133.5 days in male [114]. Adenocarcinoma that arises in virgin and breeder females as well as males was observed to be multifocal, highly fibrotic and involves the entire mammary fat pad [96, 114]. Mice carrying the PyVT transgene also show loss of lactational ability since the first pregnancy [114]. Pulmonary metastases are also observed in 94% of tumor-bearing

female mice and 80% of tumor-bearing male mice [114-116]. The Mice female offsprings were palpated every 3 days from 12 weeks of age to identify tumors.

Individual mouse was restrained by using a plastic restrainer when the tumor diameter reached 2cm for the transgenic mice or when it reached 18 weeks of age for normal mice. Anesthesia was performed by using the Ketamin-Xylazil-Zoletil cocktail dilution. 0.2ml of the anesthetic drug was administered intravenously from the mouse tail and an additional of 2ml of the drug was delivered intraperitoneally for about 2 hours of sleeping time. Fur around the breast area was shaved. The mammary tissue was harvested from the mice while they were sleeping. Mice were then killed by using drug overdose method. Excised breast specimens were cut down to an approximately 1cm x 1cm square shape with thickness of 2mm immediately after the surgery to maintain the tissue physiological activities. Tissue was carefully trimmed down to the required thickness and standardization was made by using a custom made U-shaped mold with 2mm opening. The overall process of trimming down after excision took an average time of 1 minute. A total of 24 normal and 25 cancerous breast tissue specimens were used in this study.

3.3.3 Ultrasound Measurement

In ultrasound measurement, specimens were immersed in oil that was located between the ultrasound transmitter and receiver [127]. Measurement was done in transmission mode, in which 2 ultrasound transducers were used as transmitter and receiver. The transmission mode approach gives some advantages including less complicated data and less noise [93, 127]. The distance between the ultrasound transmitter and receiver was set constant to 6mm. Ultrasound analysis was started and performed at a constant temperature of 21°C by using the insertion loss method described elsewhere previously [92-93, 96-100, 127]. Sonification was conducted from the z direction. Vegetable oil was used as medium for ultrasound propagation to prevent any leakage current from contaminating the measurement chamber and interfering the HMM magnetoacoustic voltage output [67]. A total of 15 gel samples were used in the

early part of this study and measurements were conducted once for every gel sample. In addition to that, 24 normal and 25 cancerous mice breast tissue samples were used. The biological samples were divided into 2 groups namely: the normal group and the cancerous group. Measurement was repeated for 5 times for every sample at any random position on the sample surface.

3.3.4 Magnetoacoustic voltage Measurements

The magnetoacoustic voltage measurement was made by touching the tissue surface from the x direction using the skin electrodes. Before the measurement was started, the baseline reading of the Lock-In amplifier was recorded. Baseline reading 1 was recorded when the ultrasound pulser receiver was turned off and the electrodes were placed outside the permanent magnet. Baseline reading 2 was recorded with the ultrasound pulser receiver was turned on and the electrodes were placed outside the permanent magnet. Baseline reading 3 was recorded when the ultrasound pulser receiver was turned on and the electrodes were placed inside the permanent magnet. Finally baseline reading 4 was recorded when the ultrasound pulser receiver was turned on and the electrodes were immersed in the oil inside the measurement chamber in the present of magnetic field.

The time constant of the lock-In amplifier was set to 3ms. Hence, the recorded reading of the amplifier is equal to the average Vrms of the first and second peak signals.

A total of 15 gel samples were used in the early part of this study and measurement was repeated twice for each gel. In addition to that, 24 normal and 25 cancerous breast tissue samples were used and they were divided into 2 groups namely: the normal group and the cancerous tissue group. Measurement was repeated for 5 times for every biological tissue sample at any random position on the breast tissue surface at one measurement side (side 1). After the 5^{th} measurement, the tissue orientation was changed and measurement was repeated again for 5 times (side 2).

3.4 Experimental Data Analysis

The experimental data analysis stage comprises of analysis of HMM ultrasound output and HMM magnetoacoustic voltage output. In general, the HMM ultrasound output requires further processing in Matlab to find the attenuation scale of the ultrasound wave in every sample via spectral analysis. On the other hand, the HMM magnetoacoustic voltage output does not require further processing and the measured data was read and recorded directly from the Lock In microamplifier. Then, the resulting attenuation scale and the magnetoacoustic voltage were statistically analyzed to find the mean and standard deviation for every group.

3.4.1 Ultrasound Data Analysis

The objective of processing the HMM ultrasound output was to calculate the power spectral density of the signal. It involved determination of frequency content of a waveform via frequency decomposition. The used of power spectral density as an estimates of ultrasound attenuation was reported in [92, 96-100, 127].

During the data collection stage, the HMM system recorded 10000 lengths of ultrasound signal samples by using a frequency sampling of 1 GHz in time domain. However, those 10 thousand samples were too long and only the required signals were extracted [127]. All signals were first filtered by using the Low Pass Butterworth filter to remove the unwanted signal over 15 MHz. The signals were then converted to frequency domain for analysis by using the FFT functions.

Power Spectral Density of the ultrasound signal was plotted in Matlab. The attenuation scale was calculated by subtracting the log mean power spectrum of ultrasound signal propagating through the oil without tissue by the log mean power spectrum of ultrasound signal propagating through the oil with tissue following the equation:

$$\text{Attenuation (dB)} = \log P_0 - \log P_s \qquad (14) \quad [127]$$

Where P_s is the mean squared spectrum of the ultrasound signal propagating in the medium with tissue/gel sample and P_0 is the mean squared spectrum of ultrasound signal propagating through medium without sample.

Later, the attenuation scale for the gel, normal tissue group and cancerous tissue group were exported to Microsoft Excel for statistical analysis. The statistical analysis involved the determination of mean and standard deviation for every group.

3.4.2 Magnetoacoustic Voltage Analysis

The recorded magnetoacoustic voltage data was deducted by baseline reading 4 to eliminate any voltage value that is caused by external noise. After deduction, statistical analysis involving the calculation of mean and standard deviation was conducted according to the sample group: 1) gel group, 2) normal tissue group (side 1 and side 2) and 3) cancerous tissue group (side 1 and side 2) in Microsoft excel.

3.5 Data Massaging

Data massaging involves restructuring the range of neural network input and target values between zero to one. Massaging is done due to the fact that neural network works best when all its input and output vary within the range of 0-1 [69-70] by using the following equation:

$$Massage\ Value = (Actual\ input - Minimum\ input)/(Maximum\ input - Minimum\ input) \quad (15),$$ [70].

3.6 Development of MFNN

The diagnosis of breast cancer in this study was performed by employing a Multilayer Feed Forward Neural Network (MFNN) with 2 inputs. It was trained by using the steepest descent with momentum back propagation algorithm in Matlab environment. The back propagation algorithm is the most commonly used algorithm in medical computational application as were experimented by [69-70, 75, 82].

The measurement of ANN performance was observed by using the Mean Squared Error (MSE) and total prediction accuracy of the network to the tested data. Training is best when the ANN is capable to achieve lowest MSE value. Researches perform by [69-70, 73, 75, 78] used MSE as the measurement of ANN performance.

In addition to that, each ANN configuration was tested by using the testing group data to obtain the overall prediction accuracy as were experimented by [69-70, 80-82]. By using this method, network was trained using a part of the data and the remainder was assigned as testing and validation data.

The designation of ANN in this study involves a few steps as follows:

3.6.1 Training of ANN

The training of ANN was performed in Matlab Environment. In the Neural Network Toolbox, the network was trained by using the *traingdm* algorithm with *logsig* and *purelin* transfer functions. The training process starts when the data is presented to the network by an external supervisor. The algorithm and transfer function that were employed were as follows:

3.6.1.1 Training algorithm: *Traingdm* - is a training process that employs the steepest gradient descent with momentum algorithm to allow faster convergence.

3.6.1.2 Non linear Transfer functions: *Logsig* - is the sigmoid function, whose graph is s-shaped. It is the most common form of activation function that exhibits a graceful balance between linear and nonlinear behaviour. The logsig function takes the input value between plus and minus infinity and squashes the output into the range of 0 to 1 as the input goes from negative to positive infinity [69-70, 113].

3.6.1.2 Linear transfer function: *Purelin* - is a transfer function at the end of the sigmoid neurons. Sigmoid neurons squash their output in the range of 0 to 1. Hence, purelin neurons are used to allow the network to take any output values [113].

3.6.2 Determination of Optimal Hidden Layer Size, Learning Rate, Momentum Constant and Iteration Rate of ANN.

The determination of optimal network architecture of the developed ANN was conducted systematically by varying the ANN training parameters. The training parameters include number of neuron in the hidden layer, learning rate, momentum constant and iteration rate.

During the determination process, as one parameter was being varied to find its optimum value, the other parameters were kept constant at a particular predefined value. The value of each parameter under study was considered optimum when the network is capable to produce low MSE value and high prediction accuracy to the testing data.

The determination of optimal value of each parameter was done in the sequence as follows:

3.6.2.1 Determination of optimal hidden layer size – Number of hidden neuron was varied and learning rate, momentum constant and iteration rate were kept at a predefined value of 0.1, 0.7 and 2000 respectively.

3.6.2.2 Determination of Optimal learning rate – Learning rate was varied, momentum constant and iteration rate were kept constant at a predefined value of 0.7 and 2000, and number of hidden neuron was at optimal value as obtained in the previous determination process.

3.6.2.3 Determination of optimal momentum constant – Momentum constant was varied; iteration rate was at 2000, learning rate and hidden layers were at their optimal value.

3.6.2.4 Determination of optimal iteration rate – Iteration rate was varied and the other parameters were kept constant at their optimal values

CHAPTER 4 – RESULT

This chapter compiles the final calculation and experimental result of this study. Section 4.1 shows a step by step calculation to find the value of HMM magnetoacoustic voltage. The experimental observation and result were presented in section 4.2. Section 4.3 compares the experimental result with the previous analytical calculation result. Finally, section 4.4 presents the development process of the ANN that was used for breast cancer classification.

4.1 Prediction of the HMM Voltage Output

The magnetoacoustic voltage value was calculated following the modelling and calculation condition specified in section 2.2. The calculation involved determination of the first and second peak of the magnetoacoustic voltage signal via the determination of acoustic power, ultrasound intensity and ultrasound peak pressure, particle velocity in tissue and finally strength of the Lorentz Force.

4.1.1 Calculation of acoustic power of the ultrasound circuit

In order for magnetoacoustic voltage output range to be predicted, the acoustic power of the stimulating sound wave was first calculated. For a 9.8 MHz ultrasound signal with amplitude of 400V and PRF of 5kHz, the corresponding average voltage of the signal was:

$$V_{average} = Duty\ Cycle\ x\ Peak\ Voltage = \frac{1.02e^{-7}}{2e^{-4}}\ x - 400 = -0.204\ V \qquad (6),$$

[83-84].

In which,

$Duty\ cycle, D = \frac{\tau}{T}$ (7), [83-84]

With τ=duration of an active voltage pulse from the pulser receiver unit and T is the period of the pulse. For a 9.8MHz signal,

$$\tau = \frac{1}{9.8e^{6}} = 1.02e^{-7}$$

$$T = \frac{1}{5000Hz} = 2e^{-4}$$

Therefore, the total electrical power given to the ceramic transducer was:

$$P_{electric} = \frac{V_{average}^2}{Z_t} = \frac{0.2041^2}{190\Omega} = 2.19e^{-4}\ \text{W} \quad (8), \quad [85].$$

and Z_t is the ceramic element impedance value of 190Ω at the frequency of 9.8MHz [88].

Subsequently, the delivered acoustic power to the ceramic element was determined by multiplying the electric power, $P_{electric}$ with the electroacoustic coupling constant, K_c of the ceramic element. The value of K_c is 0.8 [86-87, 18].

$$P_{acoustic} = P_{electric}\ x\ 0.8 = 1.752e^{-4}\ \text{W} \quad (9), \quad [18, 86-88].$$

4.1.2 Calculation of Ultrasound intensity

The ultrasound intensity was calculated by dividing the acoustic power of the ultrasound pulse with its beam area [86-89]. For a flat transducer, beam diameter was first calculated to find the beam area. Beam diameter was calculated following the equation:

$Beam\ Diameter = 0.2568 D_0\ x\ S_F$ (11), [90].

In which, D_0 = element diameter of the ceramic transducer of $5e^{-3}$ m and S_F = normalized focal length with its value is 1 for a flat transducer [90].

Therefore,

$$Beam\ Diameter = 0.2568 d\ x\ S_F = 0.2568(5e^{-3}) = 1.284e^{-3} m$$

This means that, its corresponding beam radius was: $6.42e^{-4}$ m.

Then, the beam area was calculated following a general equation for a round-shape area:

$$Beam\ Area = \pi\left(\frac{beam\ diameter}{2}\right)^2 = \pi\left(\frac{1.284e^{-3}}{2}\right)^2 = 1.295e^{-6} m^2$$

Finally, the acoustic intensity was obtained by dividing the acoustic power and beam area:

$$Ic = \frac{P_{acoustic}}{beam\ area} \quad (10), \quad [18, 86\text{-}89]$$

$$Ic = \frac{1.752e^{-4}}{1.295e^{-6}} = 135.29\frac{W}{m^2}$$

From the calculation, the total acoustic intensity of the beam was 135.29W/m^2 and this value is acceptable for a single element transducer since the maximum value of temporally averaged intensity limited by FDA for diagnostic, single and multi element transducer is 0.7W/cm^2 or 7000W/m^2.

The ultrasound beam with initial intensity of 135.29W/m^2 departs from the transducer's matching layer and propagates through a 4mm depth of oil. The propagation of sound wave in a highly attenuating media such as oil had causes its initial intensity to be attenuated. Previous study [117] reported that average attenuation value of edible oils at 10MHz is 59Np/m in which, equals to 5.12dB/cm. Hence, for a 4mm depth of oil, the attenuation is 2dB. However, this average value does not include the

attenuation of palm oil that is used in this study. Due to the property of highly attenuating palm oil, the attenuation value was closely approximated to -3dB.

Hence, the remaining ultrasound intensity at the time it hits the tissue surface was only 50% of its original intensity (-3dB loss =50% loss). So, the attenuated intensity value was:

$$I_{f1} = \frac{50}{100} x\ I_C = \frac{50}{100} x\ 135.29 = 67.64 \frac{W}{m^2} = 67.64 \frac{Kgm^2}{m^2 s^3}$$ [18]

4.1.3 Calculation of Peak ultrasound pressure and particle motion speed

When the ultrasound beam with intensity of I_{f1} passes a point in the tissue sample, the particles in the tissue were alternately compressed together and pulled apart leading to oscillation in the local pressure. The peak pressure P_{01}, during the passage of the pulse was calculated following the equation:

$$P_{01} = \sqrt{I\ x\ z} \qquad (12), \quad [68, 86\text{-}87, 90]$$

$$P_{01} = \sqrt{67.64x\ 1.540e^6}$$

$$= \frac{10206\ kg}{ms^2} = 10206\ \text{Pa}\ \approx 0.1\text{Bar}$$

However, this initial pressure was the total pressure that creates a longitudinal and shear wave in the breast tissue. Previous study reported that as much as 36% of ultrasound pressure is converted to the form of shear wave especially in highly elastic material such as breast cancer tissue, and the remaining is in the form of longitudinal wave [124]. Since the value of Lorentz Force is only influenced by the longitudinal wave in z direction, the final peak pressure was calculated by considering only the remaining 64% of the initial peak pressure. Therefore, the final peak pressure at the

upper tissue boundary (First boundary) to generate the first magnetoacoustic voltage peak was:

$$P_{f1} = \frac{64}{100} x\ P_0 = \frac{64}{100} x\ 10206 \frac{kg}{ms^2} = 6531.84\ \frac{kg}{ms^2}$$

Finally, the peak particle velocity V_0, which was caused by the pressure P_{f1} was calculated:

$$V_{01} = \frac{P_0}{\rho c_0} \qquad (13), \quad [68]$$

$$V_{01} = \frac{6531.84 \frac{kg}{ms^2}}{1020 \frac{kg}{m^3}\ x\ 1450 \frac{m}{s}} = 4.416e^{-3} \frac{m}{s}\ in\ z\ direction$$

Therefore, the longitudinal particle motions of an ultrasonic wave have caused the ion to oscillate back and forth in the medium with velocity V_{01}= 4.416e^{-3} m/s in z direction.

4.1.4 Determination of Lorentz Force and Magnetoacoustic voltage value

Earlier calculation shows that the ionic particle in the breast tissue moved with velocity of 4.416e^{-3} m/s. In the presence of a static magnetic field, B_0=0.25 Tesla in y direction the moving ion was subjected to the Lorentz Force.

$$F_1 = q[\ \mathbf{V_z} x\ \mathbf{B_y}] \qquad (1) \qquad [63\text{-}68]$$

The Lorentz Force separates positive and negative ions in the breast tissue creating two separate electric current densities J_0 of positive and negative ions. The first current density contained only positive ions and the second current density contained only negative ions or vice versa depending on the electromagnetic right hand rule law. Its magnitude was calculated as follows:

$F_1 = qE$

$E_1 = \mathbf{V_z} x \mathbf{B_y}$ (2), [63-68]

$J_{x1} = \sigma[\mathbf{V_z} x \mathbf{B_y}]$ (3), [63-68]

Whereby the conductivity σ value of cancerous tissue is 0.8 Sm^{-1} [22],

$J_{x1} = 0.8[4.416e^{-3}{}_z x 0.25_y]$

$J_{x1} = 8.832e^{-4}{}_x$

Hence, the resulting electric current in the breast tissue can be further calculated by integrating the current density, J_x over the ultrasound beam surface in cylindrical coordinate:

$I_1 = \int J_{x1} . dS$ (4), [63-68]

In cylindrical coordinate,

$$\begin{matrix} J_\rho \\ J_\varphi \\ J_Z \end{matrix} = \begin{bmatrix} \cos\varphi & \sin\varphi & 0 \\ -\sin\varphi & \cos\varphi & 0 \\ 0 & 0 & 1 \end{bmatrix} \begin{bmatrix} J_x \\ J_y \\ J_Z \end{bmatrix} = \begin{bmatrix} \cos\varphi & \sin\varphi & 0 \\ -\sin\varphi & \cos\varphi & 0 \\ 0 & 0 & 1 \end{bmatrix} \begin{bmatrix} J_{x1} \\ 0 \\ 0 \end{bmatrix}$$

$$I_1 = \int J_{X1}\cos\varphi_{J_\rho} - J_{X1}\sin\varphi_{J_\varphi}\, dS$$

For $J_x = 8.832e^{-4}{}_x$,

$$I_1 = \int 8.832e^{-4}\cos\varphi_{J_\rho} - 8.832e^{-4}\sin\varphi_{J_\varphi}\, dS$$

For a constant azimuthal plane cylinder, the surface, $dS = d\rho dz$. Hence,

$$I_1 = \int\int 8.832e^{-4}\cos\varphi_{J_\rho} - 8.832e^{-4}\sin\varphi_{J_\varphi}\, d\rho dz$$

$$I_1 = \int_{\rho=0}^{\rho=6.42e^{-4}} \int_{z=0}^{z=2e^{-3}} 8.832e^{-4}\cos\varphi_{J_\rho} - 8.832e^{-4}\sin\varphi_{J_\varphi}\, d\rho dz$$

In which, $\varphi = 2\pi$. Therefore cos 2Π = 1 and sin 2Π = 0. This simplifies I_1 to:

$$I_1 = \int_{\rho=0}^{6.42e^{-4}} \int_{z=0}^{z=2e^{-3}} 8.832e^{-4}\, d\rho dz$$

For a carbon fiber electrode with impedance R =10kΩ, the resulting magnetoacoustic voltage was:

$$V_1 = R \text{ x } 8.832e^{-4} \int_{\rho=0}^{6.42e^{-4}} \int_{z=0}^{z=2e^{-3}} d\rho dz)$$

$$V_1 = (10000)(8.832e^{-4})(6.42^{-4})(2e^{-3}) = 1.13e^{-5}\text{ V} \quad \text{(First peak)}$$

The calculation above shows the magnitude of the first peak that occurs at the first boundary of tissue.

Calculation of the second peak involved further estimation on the attenuation of ultrasound energy as the wave propagates further through the 2mm tissue and finally hits its lower boundary. At the first tissue boundary, the ultrasound wave intensity was 67.64W/m^2. The tissue was assumed to further attenuate sound intensity at -3dB. The assumption was made since no literature review was found on the mice breast tissue attenuation. Therefore, at the end of the tissue boundary, the remaining intensity was only 50% (-3dB loss = 50% loss) of its initial intensity. Hence, the sound intensity at the second tissue boundary was:

$$I_{f2} = \frac{50}{100} x\, I_C = \frac{50}{100} x\, 67.64 = 33.82 \frac{W}{m^2} = 33.82 \frac{Kgm^2}{m^2 s^3}$$

The intensity produces local peak pressure at:

$P_{02} = \sqrt{I\ x\ z}$ (12), [68, 86-87, 90]

$P_{02} = \sqrt{33.82x\ 1.540e^{6}}$

$= \frac{7216\ kg}{ms^2}$

From that, the longitudinal ultrasound pressure was calculated as 64% of the peak pressure:

$P_{f2} = \frac{64}{100} x\ P_0 = \frac{64}{100} x\ 7216 \frac{kg}{ms^2} = 4618.8\ \frac{kg}{ms^2}$

The final pressure induces a particle velocity of:

$V_{02} = \frac{P_0}{\rho c_0}$ (13), [68]

$V_{02} = \frac{4618.8\ \frac{kg}{ms^2}}{1020 \frac{kg}{m^3}\ x\ 1450 \frac{m}{s}} = 3.12e^{-3} \frac{m}{s}\ in\ z\ direction$

From there, the resulting negative current density for the second peak was calculated as:

$J_{x2} = \sigma[\ \mathbf{V_z} x\ \mathbf{B_y}\ ]$ (3), [63-68]

$J_{x2} = -0.8[\ 3.12e^{-3}{}_{\mathbf{z}} x\ 0.25_{\mathbf{y}}\ ]$

$J_{x2} = -6.24e^{-4}{}_{x}$

Finally, the magnitude of the second peak voltage was:

$V_2 = (10000)(-6.24e^{-4})(6.42^{-4})(2e^{-3}) = -8e^{-6}$ V (Second peak)

Finally, the output of HMM was calculated by averaging the value of the first and second peaks:

$$Vf = \frac{(V_1 + V_2)}{2} = \frac{1.13e^{-5} + -8e^{-6})}{2} = 1.64e^{-6}\ V$$

4.2 Experimental Result

The experimental result comprises of 3 subsections. The first subsection (4.2.1) compiles the result of HMM ultrasound measurement. Then, subsection 4.2.2 presents the result of HMM magnetoacoustic voltage measurement. Finally, subsection 4.2.3 compares the experimental result with the analytical calculation result presented earlier in section 4.1.

4.2.1 HMM Ultrasound Output and Determination of Attenuation Scale.

Figure 4.1 below shows the output pulse of the ultrasound pulser receiver unit. The 5077PR ultrasound pulser receiver generates a series of negative pulses for transducer excitation. In HMM, the pulser receiver sent a 400V, negative pulse at the duration of 0.1microsec to excite a ceramic transducer. The pulse generated an electromechanical resonant at the transducer ceramic element to produce an A-mode ultrasound wave at its center frequency of 9.8MHz. A-mode ultrasound is a one dimensional ultrasound signal that constitutes a graph of voltage that represents the sound wave amplitude on the y-axis, as a function of time on the x-axis. The corresponding output of the transducer is shown by figure 4.2. In the figure, an ultrasound wave at the center frequency of 9.8MHz was generated, as the highest energy of the ultrasound frequency component was found at 9.8MHz. The ultrasound wave was used to scan a set of samples and the output was further analyzed to determine the attenuation scale of ultrasound at 9.8MHz in Matlab environment.

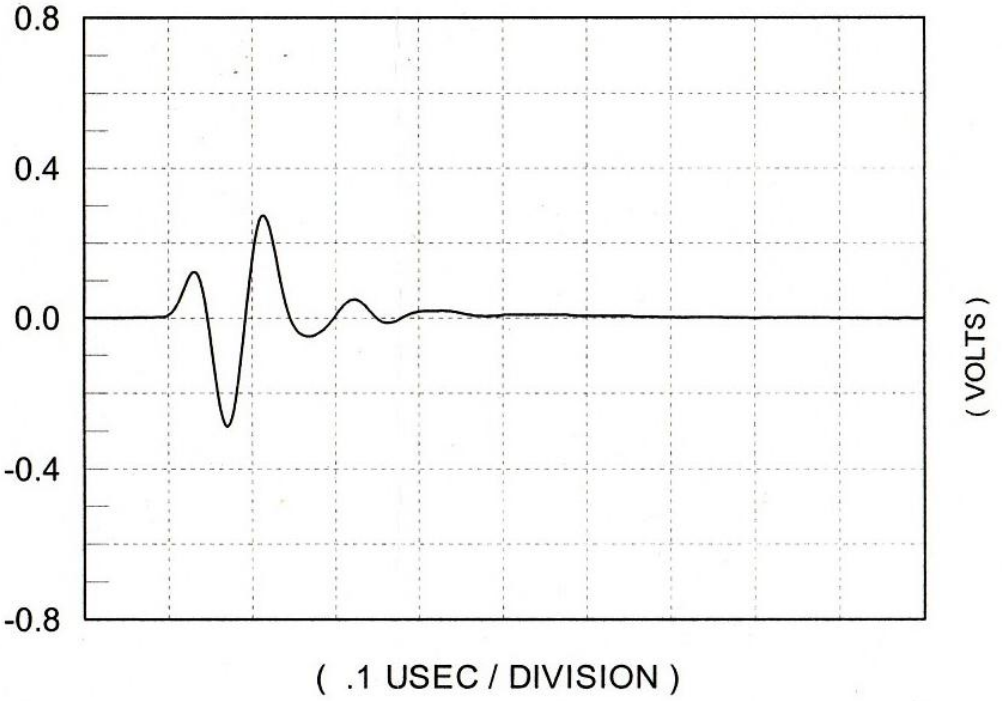

Figure 4.1: Output of the ultrasound pulser receiver unit

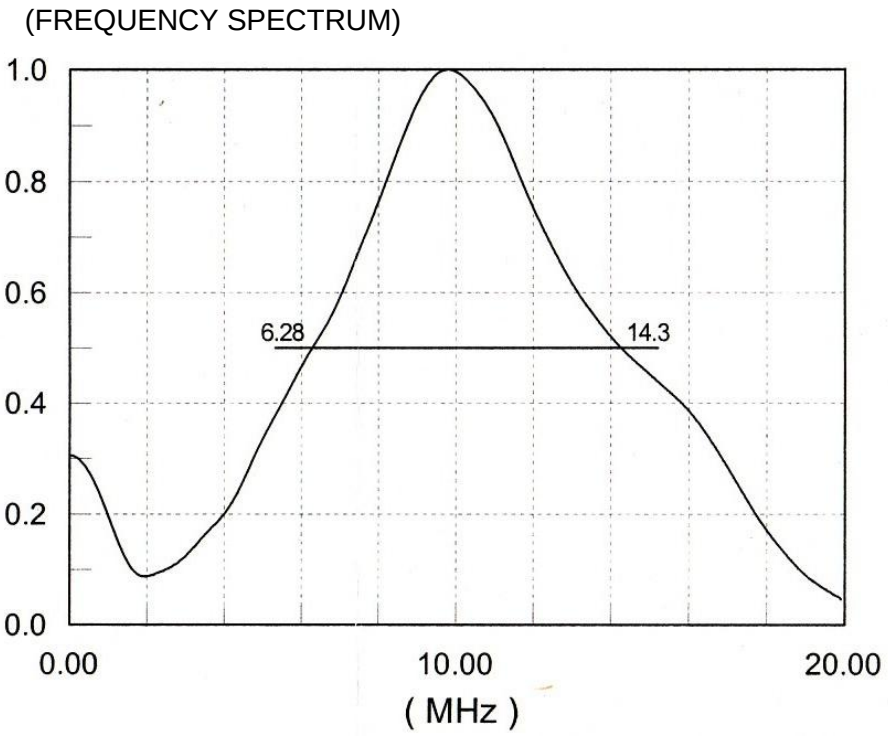

Figure 4.2: HMM transducer output

The total number of ultrasound signals that were recorded in this experiment is presented by table 4.1

No	Ultrasound signal	Quantity
1	Ultrasound signal propagating through the oil medium only	21
2	Ultrasound signal propagating through the oil medium with gel	15
3	Ultrasound signal propagating through the oil medium with normal breast tissue	106
4	Ultrasound signal propagating through the oil medium with cancerous breast tissue.	106

Table 4.1: Details of ultrasound signals recorded by HMM

Figure 4.3 shows an example of the original, one dimensional ultrasound signal output that was recorded by HMM after propagating through the oil medium without material under test. The recorded signal contains 10000 lengths of discrete data with sampling frequency of 1 Gigahertz. The first peak in figure 4.3 represents the first ultrasound wave that was sensed by the receiver transducer after propagating through the oil medium. On the other hand, the second peak represents a part of the first wave that was attenuated due to reflection. In this case, as the first sound wave hits the receiver transducer, part of it wave transmitted further and sensed by the receiver and another part was reflected back towards the transmitter. At the transmitter, the wave bounced back to the receiver and sensed. Hence, the time distance between the first and second peak indicates the time required for the wave to complete the distance between the transmitter and receiver for 2 times.

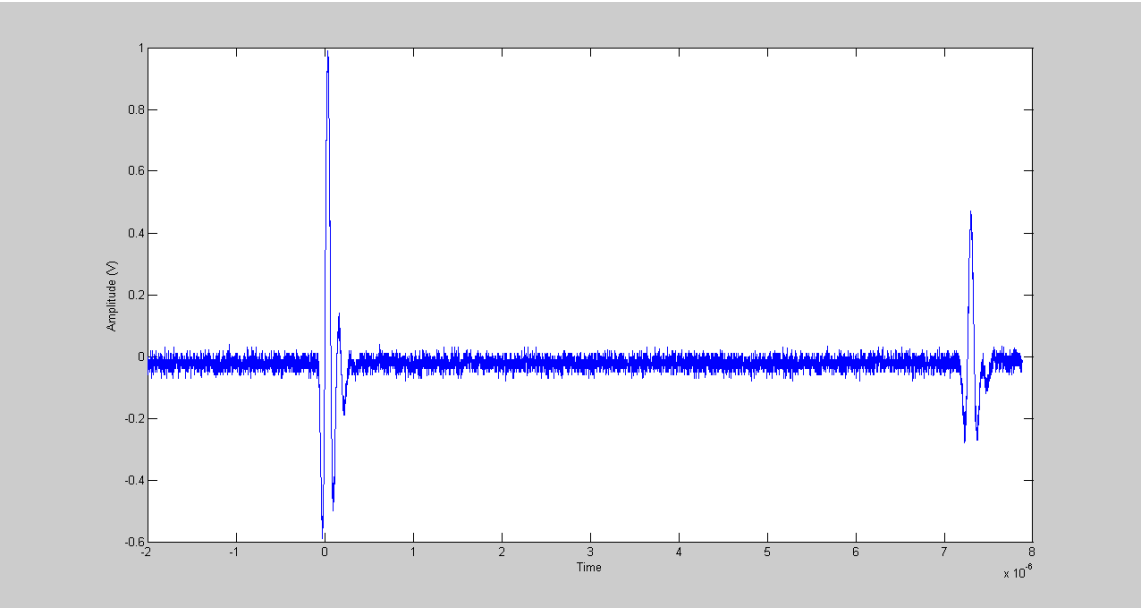

Figure 4.3: Original ultrasound signal recorded by HMM

Figure 4.4 shows the ultrasound signal that was extracted from the 10000 lengths of original data shown in figure 4.3. From the original signal, only the first peak was selected and extracted since it contains sufficient information with regards to the attenuation of ultrasound as it travels from transmitter to receiver through the oil medium. Total length of the extracted data was 601.

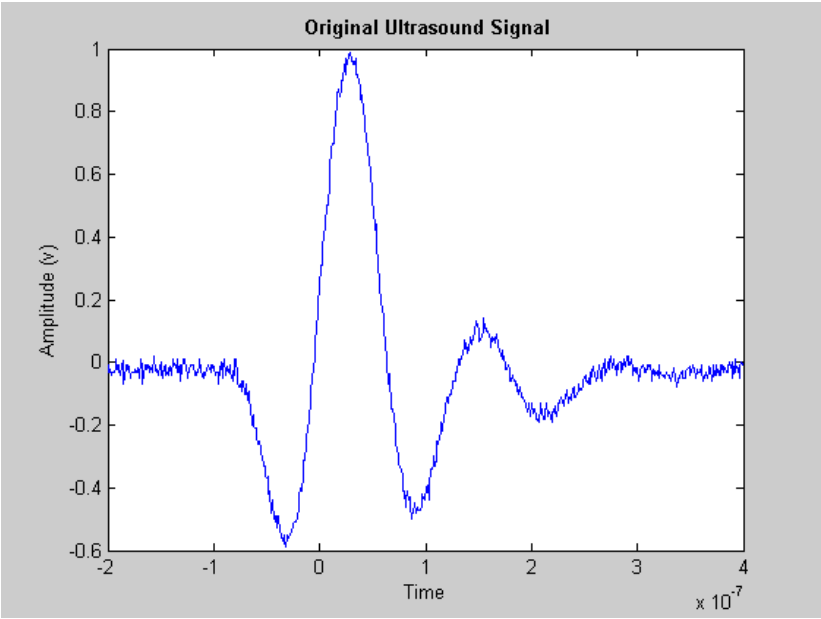

Figure 4.4: Ultrasound wave extracted by HMM after propagating through the tissue.

The extracted signal in figure 4.4 was used in the determination of ultrasound attenuation scale in this study. Attenuation is the weakening of sound wave that is characterized by the reduction in amplitude and intensity as the wave propagates through tissue [86-90, 18, 127]. It encompasses the absorption (conversion of ultrasound to heat) as it travels and the reflection and scattering as it encounters tissue interface and heterogeneous tissues [86-90, 18]. Attenuation of ultrasound is dependant to its frequency [92-93, 96-100, 127]. Higher frequency ultrasound experience more attenuation as compared to lower frequency ultrasound [92-93, 96-100, 127]. In this study, the attenuation of ultrasound propagating through a material in a medium was calculated by using the insertion loss method [92-93, 96-100, 127]. In the Insertion Loss method, attenuation of material under test was determined by subtracting the energy of ultrasound travelling through the medium with the energy of ultrasound travelling through the medium with material under test.

Later, the extracted signal in figure 4.4 was filtered by using the butterworth filter in Matlab Signal Processing Toolbox. The filtered signal was shown in Figure 4.5. Filtering involved the elimination of unwanted frequency higher than 15MHz. It also provides a smoothing effect to the signal after the elimination of high frequency signals. The Butterworth filter was chosen due to its flat passband property which is very desirable to prevent signal truncation. However, butterworth filter also has a gradual stopband that might pass a very small amount of unwanted frequency after the bandstop frequency.

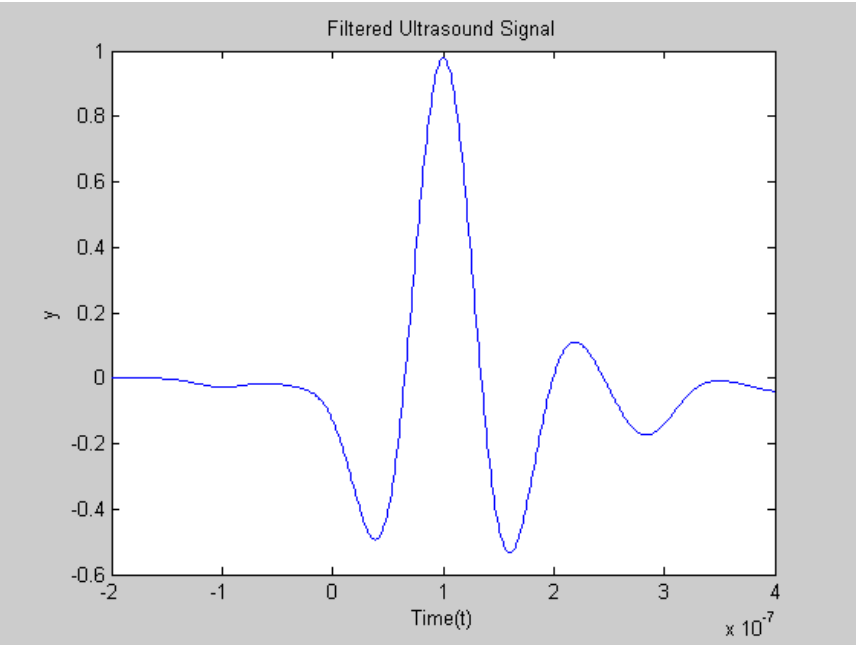

Figure 4.5: Filtered Ultrasound Signal

After filtering, the signal was converted to frequency domain by using the Fast Fourier Transform algorithm. The Fourier theorem states that any waveform in the time domain can be represented by the weighted sum of sines and cosines that represent the frequency components of the signal. FFT was chosen for its high accuracy and fast computing time. Figure 4.6 and 4.7 show the Fast Fourier Transform (FFT) of the original and the filtered signal respectively. From the figures, it can be seen that, the unwanted frequency components which is higher than 15MHz was removed after filtering process leaving only a very small amount that is very close to zero due to the gradual stopdband property of the butterworth filter.

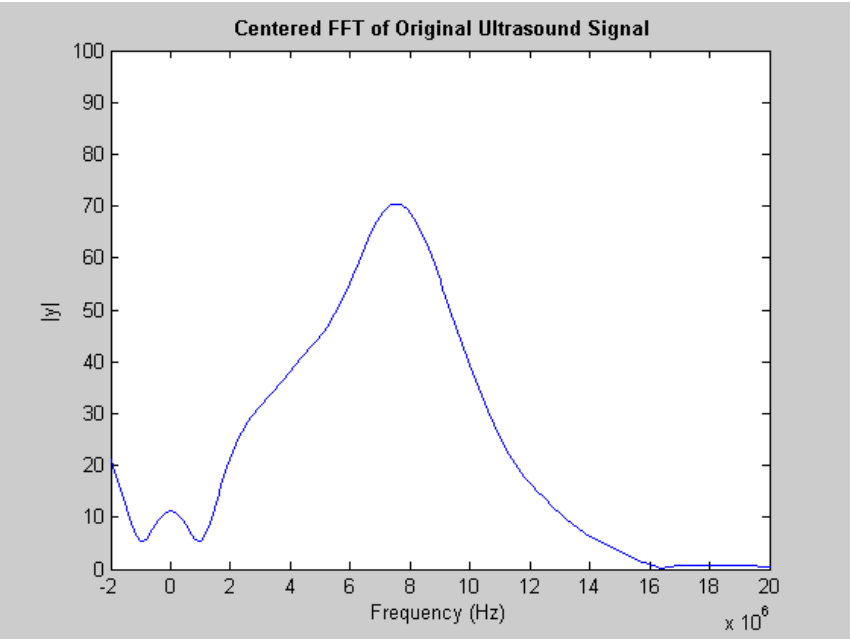

Figure 4.6: Fast Fourier Transform of the Original signal

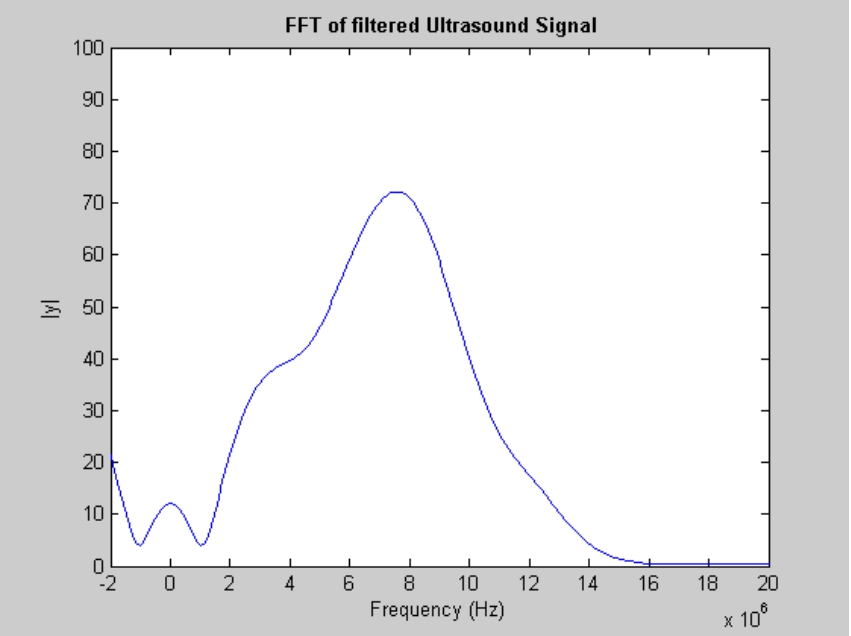

Figure 4.7: Fast Fourier Transform of the Filtered Signal

Later, the signal power was determined by calculating the signal's mean squared spectrum. Figure 4.8 illustrates the power or the mean squared spectrum of the ultrasound signal. Subsequently, the power spectral density (PSD) was calculated by converting the mean squared spectrum to its corresponding log value shown in Figure

4.9. The PSD plot shows that the highest frequency component of the ultrasound signal is at 7.8MHz though the peak energy of the input was 9.8MHz as shown by figure 4.2. This observation indicates that, most of the energy of the higher frequency components of the ultrasound wave was attenuated and hence, leaving only the energy of the lower frequency components. Finally, the attenuation scale of ultrasound at 9.8MHz was determined from the slope of PSD plot.

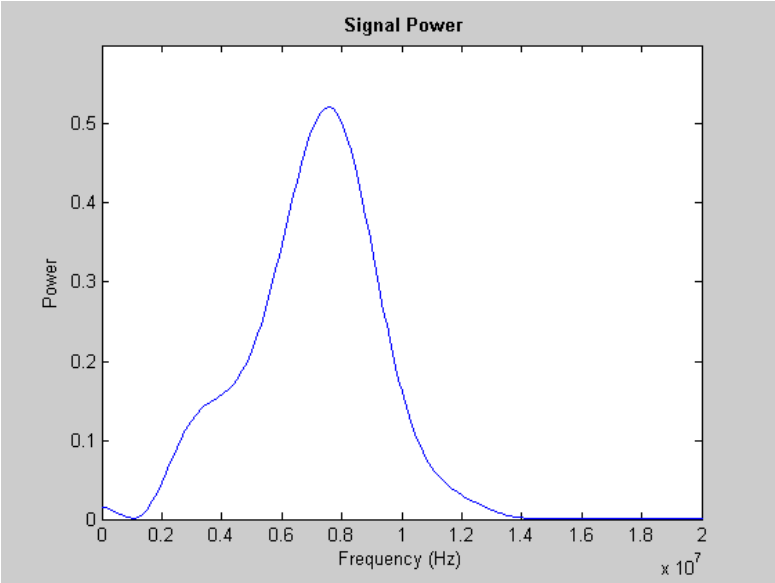

Figure 4.8: Mean squared spectrum of the ultrasound signal

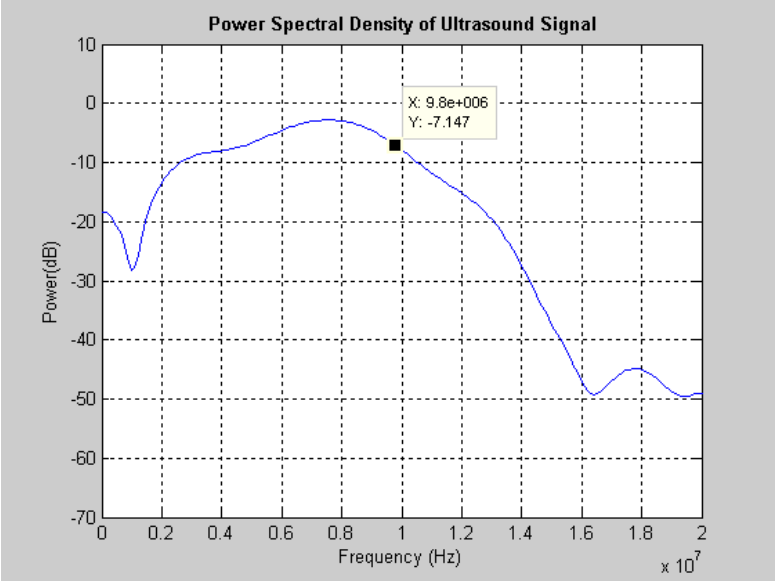

Figure 4.9: PSD of the oil signal

An Example of the PSD plot for each group is presented by Figure 4.10.

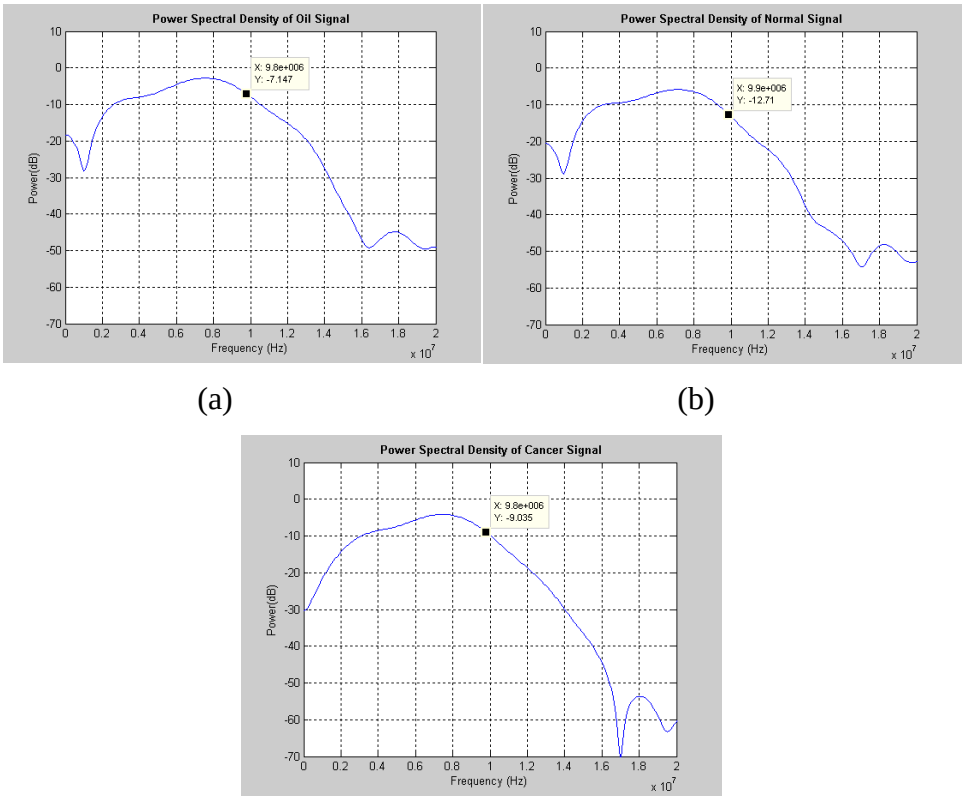

Figure 4.10: PSD of (a) oil, (b) normal tissue and (c) cancerous tissue.

The processes described above were repeated for all ultrasound signals according to their group as presented by Table 4.1. Then, the corresponding Mean and standard deviation of attenuation for each group were calculated in Microsoft Excel. The final attenuation value was calculated by subtracting the mean of power spectral density of the oil medium at 9.8MHz by the mean of power spectral density of the oil medium with material under test (gel, normal tissue and cancerous tissue) at 9.8MHz.

Table 4.2 shows the final result of ultrasound attenuation scale for each group.

Attenuation Scale Result	Output @ 9.8MHz
Attenuation of tissue mimicking gel	0.392±0.405 $dBmm^{-1}$
Attenuation of Normal Breast Tissue	2.329±1.103 $dBmm^{-1}$
Attenuation of Cancerous Breast Tissue	1.76±1.08 $dBmm^{-1}$

Table 4.2 : Attenuation scale of Hybrid Magnetoacoustic Method

From the result, it is observed that the tissue mimicking gel attenuated 0.392±0.405 $dBmm^{-1}$ of ultrasound energy which was very small compared to the attenuation of real biological tissue group. The tissue mimicking gel is an ideal representation of tissue with linear behavior. In this study, the gel was designed to have the same density with normal tissue but differs in its internal structure. The gel structure is homogenous while the real breast tissue is heterogenous. The homogenous gel structure prevents energy losses due to scattering inside the gel. Hence more ultrasound energy is likely to be preserved.

For the real biological tissue, normal tissue group attenuated the highest amount of ultrasound energy followed by the cancerous tissue group. The reason may due to the structural difference between these tissues. In general, normal breast tissue composed of loose tissue structure [92-93]. Loose structure tends to resist sound propagation and causes energy losses by absorption, in which the sound energy is converted to heat [18]. In addition to that, breast cells are heterogeneous and not uniform to each other. This heterogeneity encourages further energy losses due to scattering [18]. On the other hand, cancerous tissue group has a more compact tissue structure because more cells are piled up close to each other [6]. This structure eases ultrasound propagation and reduces energy losses by absorption. However, it still encountered energy losses from scattering process due to its heterogeneity [18]. In cancerous tissue, heterogeneity is not only contributed by the cellular difference, but also tissue structural difference in the tumor region. The tumor center usually comprises of necrotic tissue area that is more homogenous. However, the structure becomes more heterogenous towards the boundary area of tumor that is far from tumor center. This complex heterogeneity has caused the

standard deviation of the calculated attenuation scale to be higher than the homogenous structure such as in the tissue mimicking gel.

The obtained result also shows that the attenuation scale of normal and cancerous tissue is overlapping to each other. This fact had proved the complexity of breast cancer detection by using acoustic properties alone. The results were also in agreement with a previous study that reported on the attenuation of breast cancer in human breast tissue [93].

4.2.2 HMM Magnetoacoustic Voltage Output.

The magnetoacoustic voltage output measurements involved detection of as low as 0.1microvolt signal at the frequency of 9.8MHz by using the carbon fiber electrodes and lock-in amplifier. Before the magnetoacoustic voltage measurement was conducted, 4 baseline readings were recorded from the lock-in amplifier under different measurement condition. Baseline reading 1 was recorded with the ultrasound pulser receiver was turned off and the electrodes were placed outside the permanent magnet. Baseline reading 2 was recorded with the ultrasound pulser receiver was turned on and the electrodes were placed outside the permanent magnet. Baseline reading 3 was recorded when the ultrasound pulser receiver was turned on and the electrodes were placed inside the permanent magnet bore. Finally, baseline reading 4 was recorded when the ultrasound pulser receiver was turned on and the electrodes were immersed in the oil inside the measurement chamber, in the present of magnetic field. The recorded baseline readings were presented by Table 4.3

No	Data	Value (μV)
1	Baseline reading 1	2.5 - constant
2	Baseline reading 2	2.5 - constant
3	Baseline reading 3	2.6 - constant
4	Baseline reading 4	2.6 - constant

Table 4.3: Baseline reading of magnetoacoustic voltage measurements

In general, baseline reading 1 indicates the internal noise of the Lock-in amplifier and the existing noise that presents in the anechoic chamber. Baseline reading 2 indicates additional noise that may be contributed by the pulser receiver unit or leakage current from the ultrasound transducer. However, it was observed that no additional noise was recorded in baseline reading 2 as reported in [67] with the used of nonconducting oil as medium. Baseline reading 3 indicates the interference that is caused by the magnetic field to the carbon fiber electrodes. Finally, baseline reading 4 indicates the interference that was caused by the magnetic field and ultrasound leakage current that exists in the oil. However, consistent reading indicates the existing of no leakage current. To ensure that the recorded magnetoacoustic voltage data is not contaminated by any external noise, every data value was deducted by the value of baseline reading 4. The total number of magnetoacoustic voltage signals that were recorded in this experiment is presented by table 4.4

No	Type of magnetoacoustic voltage signal	Quantity
1	Magnetoacoustic voltage of tissue mimicking gel	31
2	Magnetoacoustic voltage of Normal Breast Tissue (1&2)	212
3	Magnetoacoustic voltage of Cancerous Breast Tissue (1&2)	212

Table 4.4: Total number of magnetoacoustic voltage signal recorded by HMM.

After subtraction with the baseline value, the final magnetoacoustic voltage reading for each group was statistically analyzed to find its mean and standard deviation. The result was presented in Table 4.5.

Result	Output @ 9.8MHz
Magnetoacoustic voltage of tissue mimicking gel	0.56±0.21 μV
Magnetoacoustic voltage of Normal Breast Tissue (1&2)	0.42±0.16 μV
Magnetoacoustic voltage of Cancerous Breast Tissue (1&2)	0.8±0.21 μV

Table 4.5: Magnetoacoustic voltage result at 9.8MHz

From the table, it is observed that cancerous tissue group produces the highest magnetoaocustic voltage range, followed by the gel group and finally the normal tissue group. This is due to a few reasons that include ultrasound attenuation level in tissue and the conductivity of tissue. From the ultrasound measurement result, it was noted that normal tissue group attenuated the highest ultrasound energy. In the case of large amount of attenuation, the sound energy that is left to move the particles in tissue is decreasing. Hence, the resulting particle velocity will be reduced and consequently, the value of magnetoaocustic voltage is also lower. In addition to that, the conductivity of cancerous tissue group is also higher than the normal and the gel group. Therefore, high conductivity factor contributes further to increase the value of magnetoacoustic voltage of cancerous tissue. This result proves that the resulting magnetoacoustic voltage is not absolutely related to the tissue conductivity, but also weighted by the tissue density and uniformity that influenced the ultrasound attenuation level.

In addition to that, the magnetoacoustic voltage of gel is also higher than the normal tissue though the gel was prepared to have the same conductivity with those of normal tissue. This is also due to the high energy losses encountered by normal tissue via attenuation that reduced the final voltage value though they have similar conductivity.

In addition to that, as the recorded magnetoacoustic voltage value is proportional to $\mathbf{V_0}$ and $\mathbf{B_0}$ by $v_0 \bullet B_0 \sin\theta$, the tissue surface at which the skin electrode placement is made must be set to be in 90 degrees to the magnetic field direction and the sound wave propagation. Otherwise, the magnetoacoutic voltage reading will be lower due to the angular factor θ.

The range of magnetoacoustic voltage presented in this study was also compared to previous research report that used the same experimental setting for bioelectric measurements only [63-65]. The research reported on the first peak voltage amplitude that was obtained by using 2.4Tesla and 4Tesla static magnetic field to a polycarbonate sample at 1MHz. Linear extrapolation presented by figure 4.11 shows that the resulting voltage is in the range of $6.58e^{-7}$ at the magnetic field intensity of 0.25T, which is in similar order with the current study result presented in table 4.5. However, the estimated average voltage for the study is in the order of 10^{-8}. This difference may be caused by the used of different sample material with different conductivity value and different range of stimulating ultrasound frequency that influences attenuation level. In addition to that, this research used an amplifier with maximum gain of 60dB only.

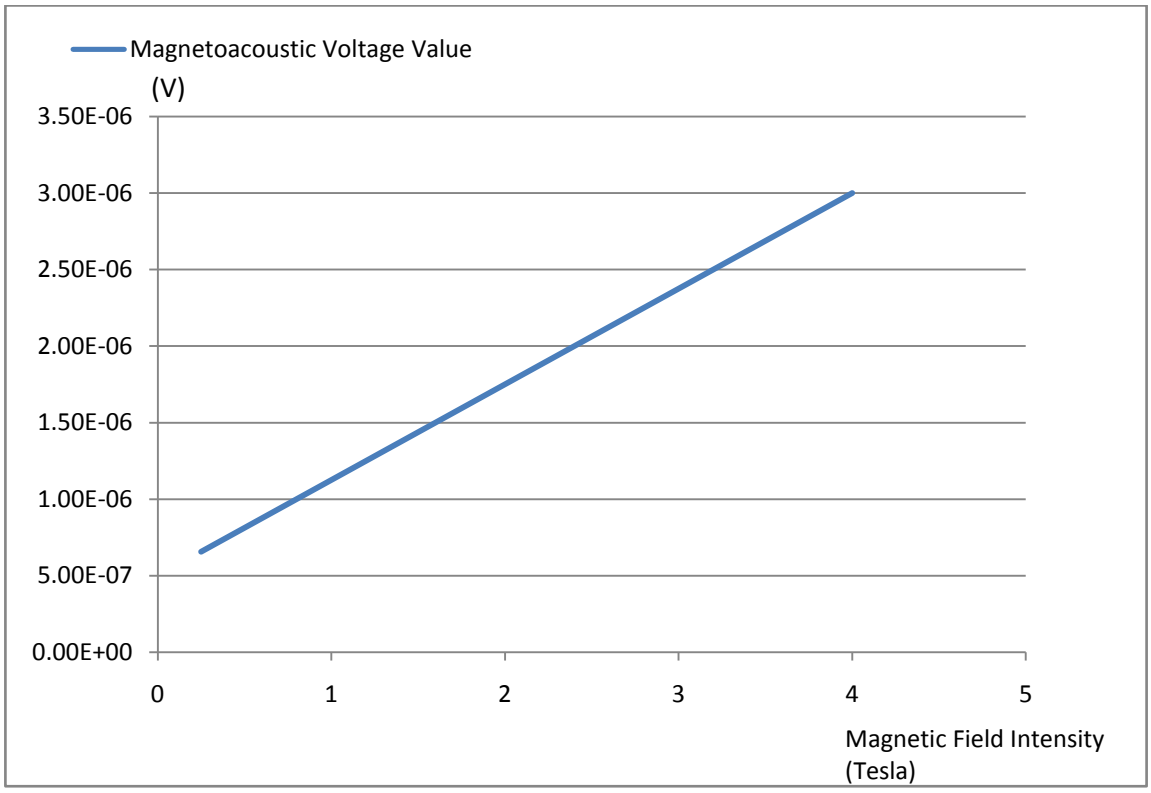

Figure 4.11: Extrapolation of magnetoacoustic voltage from previous research report.

4.3 Comparison of result from the analytical calculation.

The result of analytical calculation shows that the estimated output of HMM voltage is $1.64e^{-6}$V. However, the mean magnetoacoustic voltage value from the experiment is slightly lower than the calculated value due to a few reasons:

4.3.1 Differences in attenuation value

The amount of ultrasound attenuation of oil that was used in the calculation is -3dB. The -3dB value was taken from literature on the average attenuation value of the edible oil. However the real mean attenuation value of palm oil that was used as medium in this study was -7.17dB. Hence, this additional loss contributes further to reduce the experimental voltage value.

4.3.2 Variation in local pressure distribution that is caused by the longitudinal and shear wave. The 36% value was obtained from literature and its actual proportion in the breast tissue was not investigated.

4.3.3 Variation in the actual conductivity value of the mice breast tissue. The breast tissue is heterogenous and conductivity differences according to tissue type may occur.

4.4 Development of Artificial Neural Network (ANN) for Breast Cancer Classifications

The development of ANN comprises of a few stages that include the training stage, testing stage and validation stage. The training stage was further divided into a few steps that involved determination of optimal neuron, learning rate, momentum constant and iteration rate. The optimum ANN was then tested and validated by using the testing data and the validation data.

Before the training stage was started, the experimental database was first divided into the training, testing and validation database described by table 4.6

ANN Database	Ultrasound data		Magnetoacoustic voltage data	
	Normal	Cancerous	Normal	Cancerous
Training	68	69	68	69
Testing	28	27	28	27
Validation	10	10	10	10
Total	106	106	106	106

Table 4.6: Division of ANN database

The databases were prepared in Microsoft excel files and were exported to Matlab during the training, testing and validation process. The input database consists of 3 columns of ultrasound attenuation scale, magnetoacoustic voltage side 1 and magnetoacoustic voltage side 2. On the other hand, the output database comprises of only 1 column of training target.

A step by step process on the determination of optimal ANN for breast cancer classification was as follows:

4.4.1 Number of neuron in the hidden layer

In a multilayer feed forward neural network, the function of a hidden layer neuron is to arbitrate between the input and the output of the ANN. As the first input vector is fed into the source node in the input layer, it will be forwarded to neuron in the hidden layer. The output of a hidden layer neuron will be the input of the next hidden layer until the signal reached output layer and terminates the ANN computing. In this study, the number of neuron in the hidden layer was varied from 1 to 12 while the other parameters including learning rate, iteration rate and momentum constant were fixed to a predetermined value of 0.3, 20000 and 0.2 respectively. From figure 4.12, it can be observed that network with 12 hidden neuron produces lowest MSE value at 0.098. However, its prediction accuracy is only 89.09%. The highest prediction accuracy of 90.94% is given by 2 hidden neurons with MSE of 0.111. An increase of 0.013 in MSE has given 2% increments in prediction accuracy. Hence, hidden layer size of 2 was chosen for optimum number of neuron in the hidden layer for the ANN with slight compensation in higher MSE value.

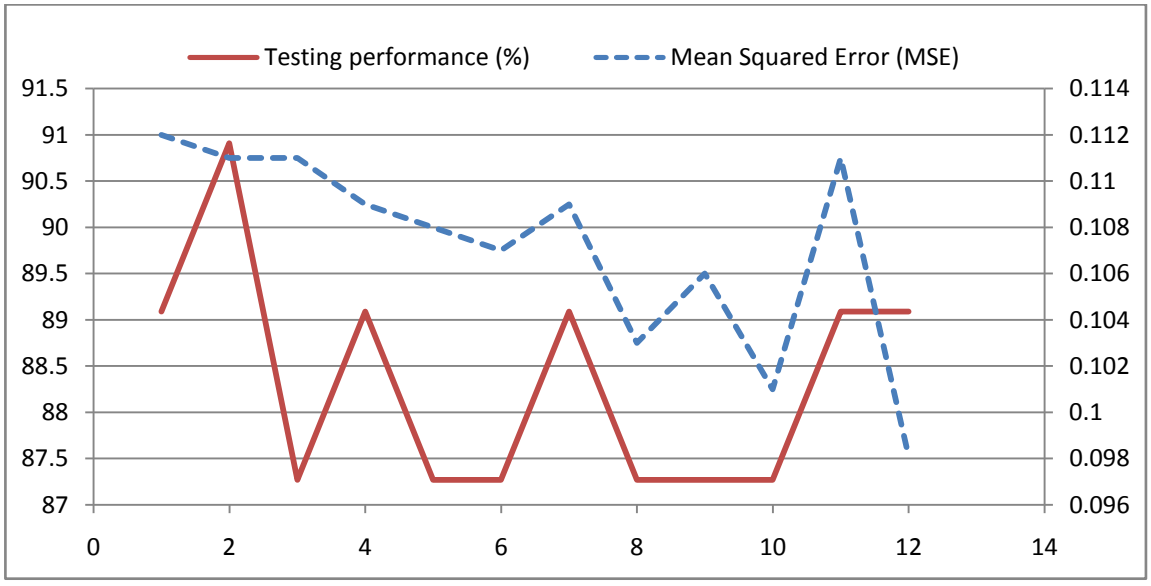

Figure 4.12: Number of neuron in the hidden layer vs Mean Squared Error (MSE) and the total accuracy (%)

4.4.2 Learning rate

The ANN learning rate was varied from 0.1 to 0.9. Training epochs and momentum constant were kept at their predetermined value of 20000 and 0.2 respectively. The number of neuron in the hidden layer was set to its optimum value of 2 neurons. Figure 4.13 shows that the lowest MSE value was achieved with learning rate of 0.1 to 0.8. In addition to that, learning rate of 0.3 to 0.8 gives the highest prediction accuracy of 90.94%. In this case, 6 optimum values of learning rate were obtained with the same MSE value and prediction accuracy. Hence, the best learning rate was chosen by testing the robustness of the ANN to validation data. The validation result shows that learning rate of 0.3 gives 90% accuracy compared to learning rate of 0.4 to 0.8 that gives 85% validation accuracy. Hence, learning rate of 0.3 was chosen as the best learning rate values.

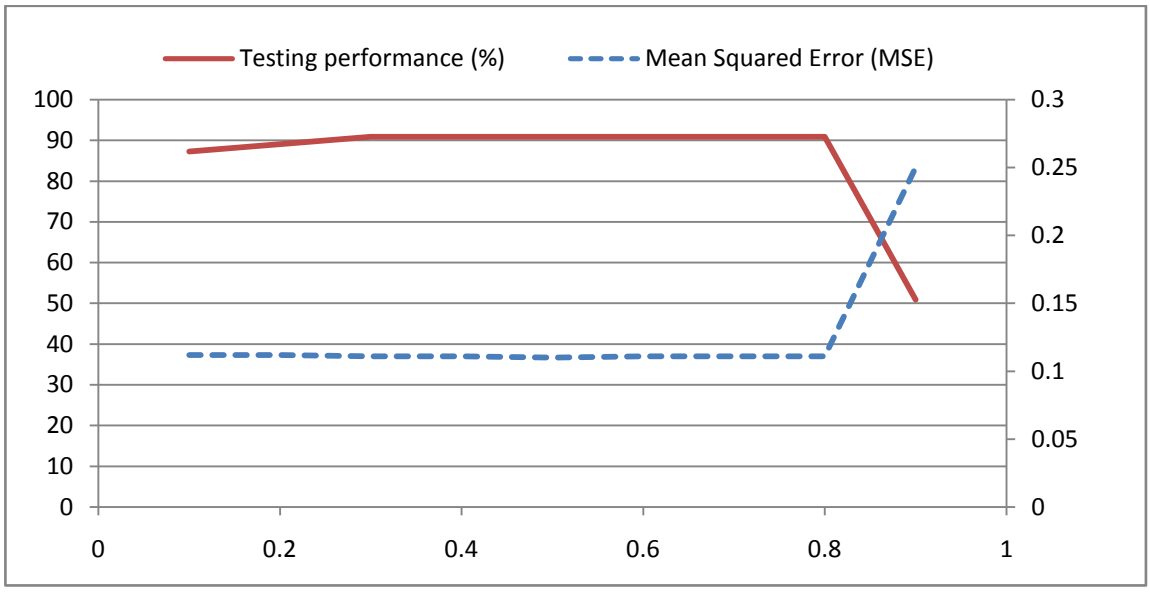

Figure 4.13: Learning rate vs Mean Squared Error (MSE) and the total accuracy (%)

4.4.3 Iteration rate.

The iteration rate was varied from 5000 to 50000 with a constant increment of 5000. Other parameters were set at their optimum value except momentum constant, which was at its predetermined value of 0.2. Figure 4.14 shows that iteration rate which is too short produces ANN with high MSE and low prediction accuracy. This indicates that the iteration rate is insufficient to allow the network to converge. It also shows that iteration rate of 20000, 40000 and 50000 give the lowest MSE value of 0.111 and the highest prediction accuracy of 90.94%. Hence, iteration rate of 20000 is chosen since this architecture produces lowest MSE and highest prediction accuracy at the shortest time interval. In addition to that, this architecture was tested to validation data and it gives the highest validation prediction accuracy of 90%.

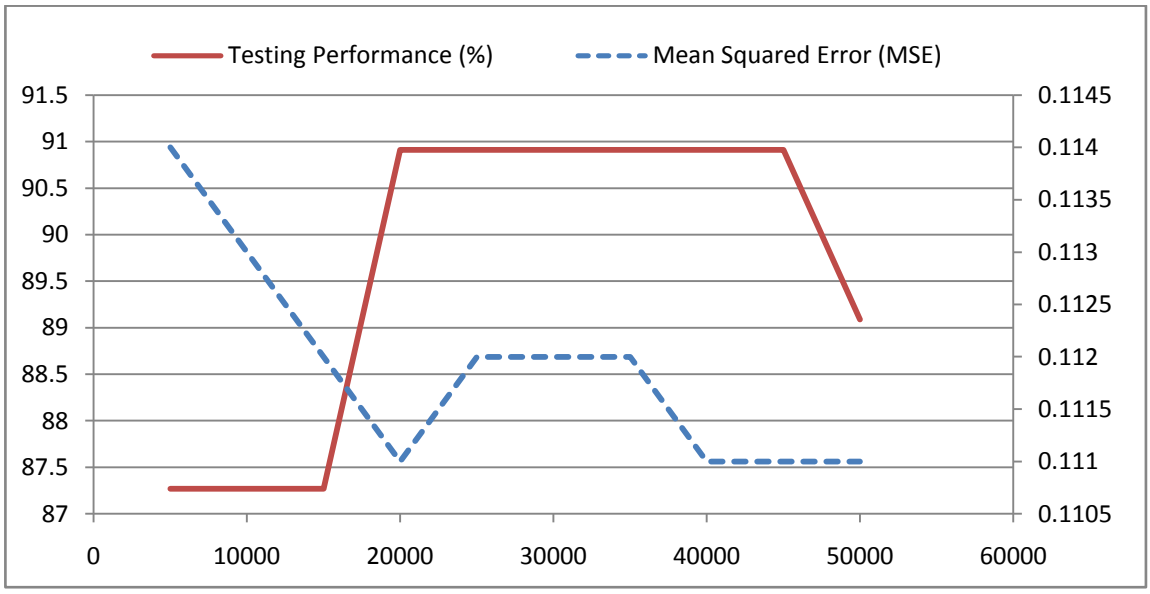

Figure 4.14: Iteration rate vs Mean Squared Error (MSE) and the total performance accuracy (%)

4.4.4 Momentum constant

The final step for the determination of optimum ANN was to find the best momentum constant for the network. The momentum constant was varied from 0.1 to 0.9 while other parameters were kept at their optimum values. Figure 4.15 indicates that momentum constant of 0.2, 0.3 and 0.5 produces network with lowest MSE value. Among that, momentum constant of value 0.3 and 0.5 gives the highest prediction accuracy on testing data. Hence, validation data was used to test the robustness of the system and the result indicates that momentum constant of 0.3 gives highest validation prediction accuracy of 90%.

Figure 4.15: Momentum constant vs Mean Squared Error (MSE) and total performance accuracy (%).

The final architecture of ANN for classifications of breast cancer in this study is 3-2-1 (3 network inputs, 6 neurons in the hidden layer, one network output) with learning rate of 0.3, iteration rate 0f 20000 and momentum constant of 0.3. Figure 5 shows the MSE of the developed ANN. In general, though the MSE of the developed ANN did not meet the error goal at 0.01, this error is acceptable for training target of 0 and 1 (0 for normal and 1 for malignancy).

The final classification performance of the optimum ANN for testing and validation data is shown in table 4.7. The result indicates that the ANN is capable to achieve 90.94% and 90% classification result for testing and validation data. This result shows the advantages of HMM output in providing additional bioelectric parameter of tissue instead of only its acoustic properties for breast cancer diagnosis consideration. The system's high percentage of accuracy shows that the output of HMM is very useful in assisting diagnosis. This additional capability is hoped to improve the existing breast oncology diagnosis. However, there result of one dimensional HMM can be further improved by using 2D HMM where classification is made image based rather than signal based.

Data	Testing Data		Validation Data	
	Normal	Malignant	Normal	Malignant
Actual Data	28	27	10	10
ANN Result	25	25	8	10
% Accuracy	89.29	92.59	80	100
% Total Accuracy	90.94		90	

Table 4.7: Classification Result of the Neural Network

CHAPTER 5 - CONCLUSION AND FUTURE WORK

5.1 Conclusion

At the end of this study, a novel tissue imaging method that is based on short pulse magnetoacoustic wave has been successfully developed. The system comprises of an ultrasound pulser receiver unit, ultrasound transducer, permanent magnet, lock in amplifier and skin electrodes. It produces 2 outputs namely: magnetoacoustic voltage output and ultrasound attenuation scale.

A series of experimental study to tissue mimicking phantom as well as to real mice breast tissue shows that, HMM is capable to access the acoustic and electric properties of tissue down to the range of microvolt. The output of HMM was further automate to develop a breast cancer diagnosis system by employing the artificial neural network. The ANN was defined by architecture 3-2-1, with learning rate of 0.3, iteration rate of 20000 and momentum constant of 0.3. The final ANN accuracy to testing and validation data was 90.94 and 90% respectively. The system's high percentage of accuracy shows that it is very useful in assisting diagnosis.

5.2 Future Work

5.2.1 Future work can be concentrated to develop a tomographic imaging system from the existing one dimensional imaging system. Development of tomographic system can be realized by using multiple ultrasound transducers and skin electrodes. However, the usage of multiple transducers and electrodes require input and output synchronization by high performance computer. The advantage of tomographic system is the capability to produce a 2D or 3D image instead of only 1D output.

5.3.2 The existing magnetoacoustic voltage can only be used to produce the boundary image of a sample. This is because; magnetoacoustic voltage peaks are generated at sample boundaries where abrupt changes in conductivity and density occur. The internal image of a sample can be mapped by integrating the HMM current output that can be measured and collected by using a current amplifier. Hence, future work can be focused in integrating the current output of HMM.

5.3.3 Future works can also involve in optimizing the ANN performance. The present accuracy of ANN to testing and validation data is 90.94% and 90% respectively. By employing optimization method such as pruning, it is desirable that the performance of the ANN to achieve 95-98%.

5.3.4 The current imaging method and its automation system are intended for breast cancer diagnosis. Future work can be concentrated on the study and development of breast cancer prognosis system that can be realized by considering breast cancer risk on asymptomatic patient.

REFERENCES

[1] Donegan, W. L. and Spratt, J. S. *Cancer of the Breast*. 5th edition. Elsevier Health Sciences, 2002.

[2] Moinfar F, *Essentials of diagnostic breast pathology A Practical Approach.* New York: Springer. 2007.

[3] Loughry, C. W. Breast volume measurements of 598 women using biostereometric analysis, *Ann Plast Surg*, 1989, 22:380-385.

[4] Malini, S. Smith, E. O. Goldzieher, J. W. Measurement of Breast Volume by Ultrasound during Normal Menstrual Cycle and with Oral Contraceptive Use, *Obstet Gynecol*, 1985, 66(4): 538-541.

[5] webmd.com, http://www.webmd.com, 8th June 2011.

[6] Locasale, J. W. and Cantley, L. C. Altered Metabolism in Cancer. *BMC Biology*, 2010, 88:88

[7] Cuzick, J. Epidemiology of Breast Cancer - Selected Highlights, *The Breast*, 2003, 12:405-411.

[8] Thomas H. V. Reeves, G. K. Key, T. Endogenous Estrogens and Postmenopausal Breast Cancer; A Quantitative Review, *Cancer Causes Control*, 1997, 8: 992-998.

[9] Cuzick, J. Powles, T. Veronesi, U. Forbes, J. Edwards, R. Ashley, S. Boyle, P. Overview of Main Outcomes in Breast Cancer Prevention Trials, *Lancet*, 2003: 361, 296-300.

[10] Warren, S. The relation of "Chronic Mastitis" to Carcinoma of the Breast, Surg Gynacol Obstet, 1940, 71:257-273.

[11] Wolfe, J. N. Albert, S. Breast Parenchymal Pattern: Analysis of 332 Incidents Breast Carcinoma, *Am J Roentgenol*, 1982, 138: 113-118.

[12] Boyd, N. F. Byng, J. W. Jong, R. A. Fishell, E. K. Little, L. E. Miller, A. B. Lockwood, G. A. Tritchler, D. L. Yaffe, M. J. Quantitative Classification of Mammographic Densities and Breast Cancer Risk: Result from the Canadian National Breast Screening Study, *J Nat Cancer Inst*, 1995, 87:670-675.

[13] Cuzick, J. Berridge, D. Whitehead, J. Mammographic Dysplasia as an Entry Criterion for Breast Cancer Prevention Trials, *Lancet*, 1991, 337: 1225.

[14] Breast cancer, Malaysia Oncology Society, malaysianoncology.org, 21st May 2011.

[15] McAree, B. O'Donnell, M. E. Spence, A. Lioe, T. F. McManus, D. T. Spence, R. A. J. Breast Cancer in Women under 40 Years of Age: A Series of 57 Cases from Northern Ireland, *The Breast*, 2010, 19:97–104

[16] Bhoo Pathy, N. Cheng, H. Y. Taib, N. A. Hartman, M. Saxena, N. Iau, P. Bulgiba, A. M. Soo, C. L. Siew, E. L. Wong, J. E. L. Verkooijen, H. M. Breast Cancer in a Multi-Ethnic Asian Setting: Results from the Singapore Malaysia Hospital-Based Breast Cancer Registry, *The Breast*, 2011, 20:75-80.

[17] Radiology Malaysia, http://www.radiologymalaysia.org, 8th June 2011.

[18] Kremkau, F. W. Diagnostic Ultrasound Principles and Instruments, 6th Edition, Saunders;Philadelphia, 2002

[19] Zou. Y. Guo, Z. A Review of Electrical Impedance Techniques for Breast Cancer Detection. *Medical engineering and physics*, 2003, 25:79-90.

[20] Pething, R. Dielectric Properties of Body Tissues. *Clin Phys Physiol Meas*, 1987,8:5-12.

[21] Blad, B. Baldertorp, B. Impedance Spectra of Tumor Tissue in Comparison of Normal Tissue: A Possible Clinical Application for Electrical Impedance Tomography. *Physiol Meas*, 1996, 17:105-115.

[22] Surowiec, A. J. Stuchly, S. S. Barr, J. B. Swarup, A. Dielectric properties of Breast Carcinoma and the Surrounding tissue. *IEEE Trans Biomed Eng*, 1988, 35: 257-263.

[23]Chaudary, S. S. Mishra, R. K. Swarup, A. Thomas, J. M. Dielectric Properties of Normal and Malignant Human Breast Tissue at Microwave and Radiowave Frequencies. *Indian J Biochem Biophys*, 1984, 21: 76-79.

[24] Fricke, H. Morse, S. The Electrical Capacity of Tumors of the Breast, *J Cancer Res*, 1926, 10: 340-376

[25] Jossinet, J. Lobel, A. Michoudet, C. Schmitt, M. Quantitative Technique for Bio-Electrical Spectroscopy, *J Biomed Eng*, 1985, 7: 289-294.

[26] Jossinet, J. Variability of Impedivity in Normal and Pathological Breast Tissue, *Med Biol Eng Comput*, 1996, 34: 346-350.

[27] AAMI. American National Standard: Safe Current Limit for Electromedical Apparatus. Document ANSI/AAMI ES1-1993. 1993.

[28] Arendt, M. L. Rudnick, J. A. Keller, P. J. Kuperwasser, C. Stroma in Breast Development and Disease, Seminar in Cell and Developmental Biology, 21(2010)11-18.

[29] Tophkhane, C. Yang, S. Zhao, Z. J. Yang, X. Cell density-dependant regulation of p73 in breast cancer cells. International Journal of Breast Oncology, 2009, 35:1429-1434.

[30] Chan, J. K. Magistris, A. Loizzi, V. Lin, F. Rutgers, J. Osann, K. DiSaia, P. J. Samoszuk, M. Mast cell density, angiogenesis, blood clotting, and prognosis in women with advanced ovarian cancer, Gynecologic Oncology, 2005, 99:20-25.

[31] Fern, A. J. Breast Cancer Treatment by Focus Microwave Thermotherapy, Jones and Bartlette Learning, 2007.

[32] Glide, C. Duric, N. Littrup, P. Novel approach to evaluating breast density utilizing ultrasound tomography. Med Phys, 2007, 34(2):744-753.

[33] Bamber, J.C. Ultrasonic Propagation Properties of the breast in Ultrasonic Examination of the breast, 1983, John Wiley and Sons.

[34] Gasparini G, Clinical significance of determination of surrogate markers of angiogenesis in breast cancer. Criticals Review in Oncology/Hematology, 2001, 37:97-114.

[35] Bachmeier, B. E. Albini, A. Vene, R. Benelli, R. Noonan, D. Weigert, C. Weiler, C. Lichtinghagen, R. Jochum, M. Nerlich, A.G. Cell density dependant regulation of matrix metalloproteinase and TIMP expression in differently tumorigenic breast cancer cell lines. Experimental Cell Research. 2005, 305: 83-98.

[36] Bissel, M. J. Radisky, D. Putting tumors in context. Nat Rev Cancer, 2001, 1:46-54

[37] Cukierman, E. A visual quantitative analysis of fibroblastic stromagenesis in breast cancer progression. J Mammary Gland Biol Neoplasia, 2004, 9:311-324.

[38] Orimo, A. Gupta, P. B. Sgroi, D.C. Arenzana- Seisdedos, F. Delaunay, T. Naeem, R. Stromal fibroblast presents in invasive human breast carcinomas promotes tumor growth and angiogenesis through elevated SDF-1/CXCL 12 Secretions. Cell, 2005, 121:335-348.

[39] Degen, M. Brellier, F. Kain, R. Ruiz, C. Terracciano, L. Orend, G. Tenascin-W is a novel marker for activated tumor stroma in low-grade human breast cancer and influences cell behavior, Cancer Res, 2007, 67:9169-9179.

[40] Ronnov-Jessen, L. Peterson, O. W. Koteliansky, V. E. Bissell, M. J. The origin of the myofibroblast in breast cancer. Recapitulation of tumor microenvironment in culture unravels diversity and implicates converted fibroblasts and recruited smooth muscle cells. J Clin Invest, 1995, 95: 859-873.

[41] Donati, M. B. Falanga, A. Pathogenetic mechanism of thrombosis in malignancy. Acta Haematol, 2001, 106(1-2):18-24.

[42] Rickles, F. R. Falanga, A. Molecular Basis for the relationship between thrombosis and cancer. Thromb Res, 2001, 102(6):V215-224.

[43] Shinoji, M. Hancock, W. W. Abe, K. Micko, C. Casper, K. A. Baine, R. M. Activation of coagulation and angiogenesis in cancer: immunohistochemical localization

in situ of clotting proteins and vascular endothelial growth factor in human cancer, Am J Pathol, 1998, 152(2):399-411.

[44] Egeblad, M. Werb, Z. New function for the matrix metalloproteinases in cancer progression. *Nat Rev Cancer*, 2002, 2:161-174.

[45] Svensson, W. E. A Review of the Current Status of Breast Ultrasound. *European Journal of Ultrasound*, 1997, 6:77-101.

[46] Laine, H. Rainio, J. Arko, H. Tukeva, T. Comparison of Breast Structure and Findings by X- Ray Mammography, Ultrasound, Cytology and Histology: a Retrospective Study. *Eur J Ultrasound*, 1995, 2:107-115.

[47] Stavros, A.T. Thickman, D. Rapp, C. L. Dennis, M.A. Parker, S. H. Sisney, G. A. Solid Breast Nodules: Use of Sonography to Distinguish between Benign and Malignant Lesions, *Radiology*, 1995, 196:132-134.

[48] Fornage, B. D. Sneige, N. Faroux, M. J. Andry, E. Sonographic Appearance and Ultrasound Guided Fine Needle Aspiration Biopsy of Breast Carcinomas Smaller than $1cm^3$. *J Ultrasound Med*, 1990, 9:559-568.

[49] Shestak K. C. Ganott, M. A. Harris, K. M. Losken, H. W. Breast Masses in the Augmentation Mammaplasy Patient: the Role of Ultrasound, *Plast Reconstr Surg*, 1993, 92:209-216.

[50] Panzarola, P. Bosso, P. Mammography and Echography in the Study of Breast Prosthesis. *Radiol Med Torino*, 1992, 83:742-744.

[51] Levine, R. A. Collins, T. L. Definitive Diagnosis of Breast Implant Rupture by Ultrasonography. *Plast Reconstr Surg*, 1991, 87: 1126-1128.

[52] DeBruhl, N. D. Gorczyca, D. P. Ahn, C. Y. Shaw, W. W. Bassett, L. W. Silicone Breast Implants: US Evaluation, *Radiology*, 1993, 189:95-98.

[53] The, W. Wilson, A. R. M. The Role of Breast Ultrasound in Breast Cancer Screening. A Consensus Statement by The European Group for Breast Cancer Screening. *European Journal of Cancer*, 1998, 34(4):449-450.

[54] Singh, K. Azad, T. Dev Gupta, G. The Accuracy of Ultrasound in Diagnosis of Palpable Breast Lump, *JK Science*, 2008, 10(4):186-188.

[55] Sehgal, C. M. Weinstein, S. P. Arger, P. H. Conant, E. F. A Review of Breast Ultrasound. *J Mammary Gland Biol Neoplasia*, 2006, 11:113-123.

[56] Stavros, A. T. *Breast Ultrasound*, Philadelphia: William and Wilkins, 2004.

[57] Bassett, L. W. Kimme-Smith, C. Sutherland, L. K. Gold, R. H. Sarti, D. King, W. 3rd Automated and Hand Held Breast Ultrasound: Effect on Patient Management. *Radiology*, 1987, 165:103-108.

[58] Arger, P. H. Sehgal, C. M. Conant, E. F. Zuckerman, J. Rowling, S. E. Patton, J. A. Inter Reader Variability and Predictive Value of US Descriptions of Solid Breast Masses: Pilot Study. *Acad Radiol* , 2001, 8:335-342.

[59] Chang J. M. Moon, W. K. Cho, N. Park, J. S. Kim, S. J. Radiologist's Performance in the Detection of Benign and Malignant Masses with 3D Automated Breast Ultrasound (ABUS), *European Journal of Radiology*, 2011, 78:99-103.

[60] Flobbe, K. Nelemans, P. J. Kessels, A. G. H. Beets, G. L. Von Meyenfeldt, M. F. Van Engelshoven, J. M. A. The Roll of Ultrasonography as an Adjunct to Mammography in the Detection of Breast Cancer: A Systematic Review, *European Journal of Cancer*, 2002, 38:1044-1052.

[61] Kuo, W. J. Chang, R. F. Moon, W. K. Computer Aided Diagnosis of Breast Tumors with Different US system, *Acad Radiol* , 2002, 9:793-799.

[62] Horsch, K. Giger, M. L. Vyborny, C. J. Venta, L. A. Performance of Computer Aided Diagnosis in the Interpretation of Lesion on Breast Sonography, *Acad Radiol*, 2004, 11:272-280

[63] Wen, H. Shah, J. and Balaban, R. S. Hall Effect Imaging. *IEEE Transactions on Biomedical EngineerinG,* 1998, 45:119-124.

[64] Wen, H. Bennett, E. Shah, J. Balaban, R. S. An Imaging Method using Ultrasound and Magnetic Field. *IEEE Ultrasonic Symposium,* 1997, 1407.

[65] Wen, H. Bennet, E. The Feasibility of Hall Effect Imaging In Humans. *IEEE Ultrasonic Symposium,* 2000, 1619.

[66] Montalibet, A. Jossinet, J. Matias, A. Cathignol, D. Interaction Ultrasound – Magnetic field: Experimental Set Up and Detection of the Interaction Current. *IEEE Ultrasonic Symposium,* 2000, 533.

[67] Su, Y. Haider, S. Hrbek, A. Magnetoacousto Electrical Tomography, A new Imaging Modality for Electrical Impedance, *IFMBE Proceeding 17,* 2007, 292.

[68] Norton S. J. Can Ultrasound be used to Stimulate Nerve Tissue? *Biomedical Engineering Online,* 2003, 2:1-9.

[69] Ibrahim, F. Prognosis of Dengue Fever and Dengue Hemorrhagic Fever Using bioelectrical Impedance, Ph.D Thesis, Department of Biomedical Engineering, Faculty of Engineering, University of Malaya; 2005.

[70] Ibrahim, F. Faisal, T. Mohamad Salim, M. I. Taib, M. N. Non Invasive Diagnosis of Risk in Dengue Patients Using Bioelectrical Impedance Analysis and Artificial Neural Network, *Med Biol Eng Compute* , 2010, 48: 1141-1148.

[71] U beyli, D. E. Implementing Automated Diagnostic System for Breast Cancer Detection. *Expert System with Application,* 2007, 33:1054-1062.

[72] Introduction to Artificial Neural Network, IEEE 1995, 08186 – 7085 – 1/95.

[73] Haykin, S. Neural Networks: A Comprehensive Foundation, New York; McMillan, 1994.

[74] Sun, M. Sclabassi, R. J. The Forward EEG Solutions can be computed using Artificial Neural Networks. *IEEE Transactions on Biomedical Engineering*, 2000, 47: 1044-1050.

[75] John, T. Wei, Z. Z. Barnhill, S. D. Madyastha, R. Understanding Artificial Neural Networks and Exploring their Potential Applications for the Practicing Urologist. *Urology*, 1998, 52:161-172

[76] Haselsteiner, E. Pfurtscheller, G. Using Time-Dependent Neural Networks for EEG Classification. *IEEE Trans Rehabil Eng*, 2000, 8:457–463.

[77] Negnevitsky, M. Artificial Intelligence, A Guide to Intelligent System. 1st Edition, Pearson Education, 2002, ISBN: 0201711591

[78] Sinha, S. K. Fieguth, P. W. Projection Neural Network Model for Classification of Pipe Defects. *J Autom Constr*, 2005, 15(1):73.

[79] Basheer, I. A. Hajmeer, M. Artificial Neural Networks: Fundamentals, Computing, Design, and Application. *J Microbiol Methods*, 2000, 43:3–31.

[80] Lammers, R. I. Hudson, D. L. Seaman, M. E. Prediction of Traumatic Wound Infection with a Neural Network-Derived Decision Model, *American Journal of Emergency Medicine*, 2003, 21(1):

[81] Subasi, A. Automatic Recognition of Alertness Level from EEG by using Artificial Neural Network and Wavelet Coefficient, *Expert System with Applications*, 2005, 28: 701-711.

[82] Joo, S. Y. Moon, W. K. Kim, H. C. Computer Aided Diagnosis of Solid Breast Nodules on Ultrasound with Digital Image Processing and Artificial Neural Network, IEEE , 2004, 0 - 7803 - 8439 - 3/04

[83] Patrick, D. R. Fardo, S. W. *Understanding AC Circuit*, Woburn; Butterworth-Heinemann, 2000, p4

[84] Meade, R. L. Diffenderfer, R. *Foundation of Electronic Circuit and Devices*, 4th Edition, New York;Thomson, 2003, p375

[85] Dunn, P. F. *Measurement and Data Analysis for Engineering and Science*, 2nd Edition, Florida; CRC Press, p73, 2010.

[86] Szabo, T. L. *Diagnostic Ultrasound Imaging: Inside Out*, London; Academic Press, 2004

[87] Hendee, W. R. Ritenour, E. R. Medical Imaging Physics, 4th Edition, New York; Wiley Liss, 2002.

[88] Guo, H. Cannata, J. M. Zhou, Q. Kirk Shung, K. Design and Fabrication of Broadband Graded Ultrasonic Transducers with Rectangular Kerfs, *IEEE Trnas Ultrason Ferroelectr Freq Control*, 2005, 52(11): 2096-2102.

[89] Azhari, H. *Basics of Biomedical Ultrasound for Engineers*, New Jersey; John Wiley and Sons, p55, 2009.

[90] *Olympus Ultrasonic Transducers Technical Notes*, Olympus-ndt, 2006.

[91] Hoskins, P. R. Martin, K. Thrush, A. *Diagnostic Ultrasound: Physics and Equipment*, Cambridge University Press, Cambridge, P.20, 2010.

[92] Edmonds, P. D. and Mortensen, C. L. Ultrasonic Tissue Characterization for Breast Biopsy Specimen, *IEEE Ultrasonic Symposium*, p 915, 1987.

[93] Landini, L. and Sarnelli, S. Evaluation of the Attenuation Coefficient in Normal and Pathological Breast Tissue. *Medical and Biological Engineering and Computing* , 1986, 24:243-247.

[94] Li, X. Xu, Y. and He, B. A phantom study of magnetoacoustic tomography with magnetic induction (MAT-MI) for imaging electrical impedance of biological tissue, *J Appl Phys*, 2006: 99(6):066112.

[95] Xia, R. Li, X. He, B. Magnetoacoustic tomography of biological tissue with magnetic induction, Proceedings of NFSI & ICFBI, 2007.

[96] Ye S. G. Harasiewicz, K. A. Pavlin, C. J. and Foster, F. S. Ultrasound Characterization of Normal Ocular

Tissue in the Frequency Range from 50 MHz to 100MHz. *IEEE Transactions on Ultrasonics, Ferroelectrics, and Frequency Control*, 1995, 42(1):

[97] Iwamoto, T. Saijo, Y. Hozumi, N. Kobayashi, K. Okada, N. Tanaka, A and Yoshizawa, M. High Frequency Ultrasound Characterization of Artificial Skin. *30th Annual International IEEE EMBS Conference*, Vancouver, British Columbia, Canada, August 20-24,

2008.

[98] Lebertre**,** M**.** Ossant, F. Vaillant, L. Diridollou, S. Patat, F. Human Dermis Ultrasound Characterization: Backscattering Parameters Between 22-45 MHz. *2000 IEEE Ultrasonic Symposium*.

[99] Raju, B. I. and Srinivasan, M. A. Characterization of human fingertip and forearm skin using attenuation coefficient of high frequency ultrasound. *IEEE Ultrasonic Symposium, 2000.*

[100] Alacam, A. Yazici, B. Bilgutay, N. Breast tissue characterization based on ultrasound RF Echo Modeling and tissue morphology. *Proceeding of 25th Annual International Conference of the IEEE EMBS*, 2003.

[101] NHS breast screening programmes. Breast cancer, http://www.cancerscreening. nhs.uk/breastscreen/breastcancer.html#incidence. (4th July 2011).

[102] Sim, X. Ali, A. Wedren, S. Goh, D. L. M. Tan, C. S. Reilly, M. et al. Ethnic differences in time trend of female breast cancer incidence: Singapore. *BMC Cancer*, 2006, 6(261).

[103] Medina, V. M. Laudico, A. Mirasol-Lumague, M. R. Brenner, H. Redaniel, M. T. Cumulative incidence trends of selected cancer sites in a Philippine population from 1983 to 2002: a joinpoint analysis. *Br J Cancer*, 2010;102(9):1411e4.

[104] Anderson, M. E. Soo, M. S. C. Trahey, G. E. Optimizing Visualization for Breast Microcalcifications, *IEEE Ultrasonic Symposium*, 2000, 1315-1320.

[105] Horsch, K. Giger, M. L. Vyborny, C. J. Venta, L. A. Performance of computer-aided diagnosis in the interpretation of lesions on breast sonography. *Acad Radiol,* 2004;11:272–280.

[106] Shankar, P. M. Dumane, V. A. Piccoli, C. W. Reid, J. M. Forsberg, F. Goldberg, B. B. Classification of breast masses in ultrasonic B mode images using a compounding technique in the Nakagami distribution domain. *Ultrasound Med Biol*, 2002;28:1295–1300.

[107] Sahiner, B. Chan, H. P. Roubidoux, M. A. Helvie, M. A. Hadjiiski, L. M. Ramachandran, A. et al. Computerized characterization of breast masses on three-dimensional ultrasound volumes. *Med Phys*, 2004;31:744–754.

[108] Dumane, V. A. Shankar, P. M. Piccoli, C. W. Reid, J. M. Forsberg, F. Goldberg, B. B. Computer aided classification of masses in ultrasonic mammography. *Med Phys*, 2002, 29:1968–1973.

[109] Chen, C. M. Chou, Y. H. Han, K. C. Hung, G. S. Tiu, C. M. Chiou, H. J et al. Breast lesions on sonograms: computer-aided diagnosis with nearly setting-independent features and artificial neural networks. *Radiology* 2003, 226:504–514.

[110] Singh, K. Azad, T. Dev Gupta, G. The Accuracy of Ultrasound in Diagnosis of Palpable Breast Lumps, JK Science, 2008,10(4): 186-188

[111] Weinstein, S. P. Seghal, C. M. Conant, E. F. Patton, J. A. Microcalcifications in breast tissue phantoms visualized with acoustic resonance coupled with power Doppler US: initial observations. *Radiology* 2002, 224:265–269.

[112]Alizad, A. Fatemi, M. Wold, L. E. Greenleaf, J. F. Performance of vibro-acoustography in detecting microcalcifications in excised human breast tissue: a study of 74 tissue samples. *IEEE Trans Med Imag,* 2004, 23:307–312.

[113] MATlab ANN Toolbox

[114] JAX Mice Database: MMTV-PyVT strain, The Jackson Laboratory, USA. 5th September 2010. http://jaxmice.jax.org/strain/

[115] Bugge T H, Lund L R, Kombrink K K, Nielsen B S, Holmback K, Drew A F, Flick M J, Witte D P, Dano K, Degen J L, 1998, "Reduced metastasis of polyoma virus middle T antigen-induced mammary cancer in plasminogen- deficient mice", *Oncogene*,16.

[116] Guy C T, Cardiff R D, Muller W J, 1992, "Induction of Mammary Tumors by expression of polyomavirus middle T oncogene: a transgenic mouse model for metastatic disease", *Mol Cell Biol*, 12(3).

[117] Chanamai, R. and McClements, D. J. Ultrasonic attenuation of Edible oils, JAOCS, 1998, 75(18): 1446-1447.

[118] Crespi, F. England, T. Ratti, E. Trist, D. G. Carbon fibre micro-electrodes for concomitant in vivo electrophysiological and voltammetric measurements: no reciprocal influences. Neurosci Lett, 1995;188:33–6.

[119] Dressman, S. F. Peters, J. L. Michael, A. C. Carbon fiber microelectrodes with multiple sensing elements for in vivo voltammetry. J Neurosci Methods, 2002;119:75–81.

[120] Shyu, B. C. Lin, C. Y. Sun, J. J. Sylantyev, S. Chang, C. A method for direct thalamic stimulation in fMRI studies using a glass-coated carbon fiber electrode, Journal of Neuroscience Methods, 2004, 137:123–131

[121] Austin, V. C. Blamire, A. M. Grieve, S. M. O'Neill, M. J. Styles, P. Matthews, P. M. Sibson, N. R. Differences in the BOLD fMRI response to direct and indirect cortical stimulation in the rat. Magn Reson Med 2003;49:838–47.

[122] Lin, J. Sun, S. Chen, C. Chang, W. Hou, B. Shyu, B. C. A fMRI study of the anterior cingulate cortex activations during direct electrical stimulation of the medial thalamus in rats. In: Proceedings of the 10th World Congress on Pain (Abstract); 2002. p. 48

[123] Stanford Research System, User's Manual, SR844 RF Lock In amplifier, 1997.

[124] White, P. J. Clement, G.T. and Hynynen, K. Longitudinal and shear mode ultrasound propagation in human skull bone, *Ultrasound Med Biol*. 2006 July ; 32(7): 1085–1096.

[125] Mohamad Salim, M. I. Tumiran, M. A. Makhtar, S. N. Rosidi, B. Ariffin, I. Ahmad, A. H. Supriyanto, E. Hybrid Magnetoacoustic Method for Breast Tumor Detection: An In-Vitro and In-vivo Modelling and Analysis. *WSEAS Transactions on Information Science and Applications,* 2010, 7(8): 1048-1057.

[126] Mohamad Salim, M. I. Tumiran, M. A. Makhtar, S. N. Rosidi, B. Ariffin, I. Ahmad, A. H. Supriyanto, E. Quantitative analysis of Hybrid Magnetoacoustic Method for Detection of normal and pathological Breast Tissue. *Proceeding of 12th WSEAS International Conference on Automatic Control, Modelling and Simulation*, pg 144-149, 2010

[127] Mohamad Salim, M. I. Ahmmad, S. N. Z. Rosidi, B. Ariffin, I. Ahmad, A. H. Supriyanto, E. Measurements of Ultrasound Attenuation for normal and pathological mice breast tissue Using 10MHz Ultrasound Wave, *Proceeding of The 3rd WSEAS International Conference on Visualization, Imaging and Simulation* (VIS'10), November 2010, Faro, Portugal.

APPENDIX A

Matlab Coding for attenuation Calculation

```
clc;
clear all;
close all;


%open and declare data in pressure file
display('choose file croping to open:');
%sprintf('%s', 'choose file croping to open:')
filename = input('Record name: ', 's');
fid2 = fopen(filename, 'r');
data2 = textscan(fid2, '%f %f');
t=data2{1};
p=data2{2};
%figure;plot(t,p);
%pause

fs=1e9;
%open and declare data in pressure file
p=data2{2};
m = length(p);           % Window length
n1 = pow2(nextpow2(m));  % Transform length
n=10000;
%%%%%%%%%%%%%%%%%%%%%%%%%%%%%%%%%%%%%%%%%%%%%%%%%%%%%%%%%%%%%%%%%%%%%%%
%%%%
%%%%%%%%%%%%%%%%%%%% before filter
%%%%%%%%%%%%%%%%%%%%%%%%%%%%%%%%%%%%%%%%%%%%

f = (0:n-1)*(fs/n);      % Frequency range
y = fft(p,n);            % DFT

%figure;plot(f,abs(y));xlabel('Frequency (Hz)');
ylabel('|y|');title('{\bf Periodogram-before filter}'),axis([-20e5 20e6
0 8]);
%pause;
%%%%%%%%%%%%%%%FFTSHIFT%%%%%%%%%%%%%%%%%%%%%%%%%%%%

f0 = (-n/2:n/2-1)*(fs/n);  % 0-centered frequency range
y0 = fftshift(y);          % Rearrange y values
y1=abs(y0);

%figure;plot(f0,y1);xlabel('Frequency (Hz)'); ylabel('|y|');title('{\bf
centered Periodogram-before filter}')
%axis([-20e5 20e6 0 100]);
%pause;


%%%%%%%%%%% filter signal %%%%%%%%%%%%%%%%%%%%%
```

```
s=filter(filterdua,p);

%%%%%%%%%%%%%%%%%%%%%%%%%%%%%%%%%%%%%%%%%%%%%%%%%%%%%%%%%%%%%%%%%%%%%%%%%%%%
%%%%% create fft using p2 %%%%%%%%%%%%%%%%

g = fft(s,n);           % DFT
g0 = fftshift(g);          % Rearrange y values
power1 = g0.*conj(g0)/n;   % or power =(abs(g0).^2)/n; Power of the DFT


%figure;plot(f0,abs(g0));xlabel('Frequency (Hz)');
ylabel('|y|');title('{\bf FFT after filter}');
%axis([-20e5 20e6 0 100]);%pause;
%figure;plot(f0,power1);xlabel('Frequency
(Hz)');ylabel('Power');title('{\bf Signal Power after filter}');
%axis([0 20e6 0 0.6])

%pause;


ydb1=pow2db(power1);
figure;
plot(f0,ydb1);axis([0 20e6 -70 10]);grid on;
xlabel('Frequency (Hz)');ylabel('Power(dB)');title('{\bf Power spectral
density-after filter}')

%pause;
%%%%%%%%%%After filter-signal in time domain%%%%%%%%%%

t1= min(t):1/fs:max(t);
Y=ifft(g);

Y=real(Y);
k0=size(t1);
k=size(t1,2);
%k=k-1
%figure;plot(t1,Y(1:k)),xlabel('Time(t)');ylabel('y');title('After
filter (time domain)');
```

Filter coding

```
function Hd = filter2
%FILTER2 Returns a discrete-time filter object.

%
% M-File generated by MATLAB(R) 7.6 and the Signal Processing Toolbox
6.9.
%
% Generated on: 16-Jan-2011 20:11:50
%
```

```
% Butterworth Lowpass filter designed using FDESIGN.LOWPASS.

% All frequency values are in MHz.
Fs = 1e9;  % Sampling Frequency

N  = 10;        % Order
Fc = 15000000;  % Cutoff Frequency

% Construct an FDESIGN object and call its BUTTER method.
h  = fdesign.lowpass('N,Fc', N, Fc, Fs);
Hd = design(h, 'butter');

% [EOF]
```